BRIEF DEFINITIVE REPORT

A human mutation in STAT3 promotes type 1 diabetes through a defect in CD8+ T cell tolerance

Jeremy T. Warshauer[1,3]* , Julia A. Belk[5]* , Alice Y. Chan[7] , Jiaxi Wang[1] , Alexander R. Gupta[4] , Quanming Shi[6] , Nikolaos Skartsis[3] , Yani Peng[4] , Jonah D. Phipps[1] , Dante Acenas[7] , Jennifer A. Smith[1] , Stanley J. Tamaki[4] , Qizhi Tang[4] , James M. Gardner[1,4] , Ansuman T. Satpathy[6] , and Mark S. Anderson[1,2,3]

Naturally occurring cases of monogenic type 1 diabetes (T1D) help establish direct mechanisms driving this complex autoimmune disease. A recently identified de novo germline gain-of-function (GOF) mutation in the transcriptional regulator STAT3 was found to cause neonatal T1D. We engineered a novel knock-in mouse incorporating this highly diabetogenic human STAT3 mutation (K392R) and found that these mice recapitulated the human autoimmune diabetes phenotype. Paired single-cell TCR and RNA sequencing revealed that STAT3-GOF drives proliferation and clonal expansion of effector CD8+ cells that resist terminal exhaustion. Single-cell ATAC-seq showed that these effector T cells are epigenetically distinct and have differential chromatin architecture induced by STAT3-GOF. Analysis of islet TCR clonotypes revealed a CD8+ cell reacting against known antigen IGRP, and STAT3-GOF in an IGRP-reactive TCR transgenic model demonstrated that STAT3-GOF intrinsic to CD8+ cells is sufficient to accelerate diabetes onset. Altogether, these findings reveal a diabetogenic CD8+ T cell response that is restrained in the presence of normal STAT3 activity and drives diabetes pathogenesis.

Introduction

Type 1 diabetes (T1D) is caused by a breakdown of immune self-tolerance that leads to the T cell–mediated destruction of pancreatic β cells and results in absolute insulin deficiency and hyperglycemia. Hallmarks of this autoimmune disease include the presence of insulitis and islet autoantibodies (Gepts, 1965; Gepts and De Mey, 1978). Genome-wide association studies show that T1D is a polygenic disease with the majority of genetic risk attributable to HLA alleles within the MHC region (Erlich et al., 2008). Numerous other susceptibility alleles (e.g., *INS*, *CTLA4*, *STAT3*, *IL6R*; Ferreira et al., 2013; Fung et al., 2009; Sharma et al., 2018; Wang et al., 2014) have been identified from genome-wide association studies and help estimate individual risk, but ultimately additional functional studies are required to elucidate the cellular and molecular bases of these associations with disease. Naturally occurring cases of monogenic T1D, although rare (i.e., loss-of-function mutations in *AIRE* and *FOXP3*), have been most informative for understanding how central and peripheral mechanisms of immune tolerance break down and for suggesting new opportunities for therapeutic interventions (Warshauer et al., 2020).

Recent large-scale sequencing efforts in genetics have identified naturally occurring gain-of-function (GOF) mutations in the gene *STAT3* as a novel cause of monogenic diabetes (Flanagan et al., 2014; Velayos et al., 2017). However, it remains unclear how excessive STAT3 signaling leads to T1D. One challenge in studying STAT3 stems from its ubiquitous expression and pleiotropic functions in diverse cell types. Within the immune system, the JAK/STAT signaling pathway regulates transcription in response to extracellular cues from cytokines. STAT3 is a transcription factor that regulates the expression of genes associated with cell survival, proliferation, activation, and differentiation (O'Shea and Plenge, 2012). Outside of the immune system and directly within pancreatic cells, STAT3 plays a role in islet development as well as insulin secretion (Gorogawa et al., 2004; Saarimäki-Vire et al., 2017; Velayos et al., 2017). Previous work has proposed multiple conflicting hypotheses regarding the relevant cell types involved in the development of diabetes caused by STAT3-GOF, such as an islet-intrinsic effect or perturbing the regulatory T (T reg)/T helper type 17 (Th17) cell balance within the CD4+ T cell compartment (Fabbri et al.,

2019; Milner et al., 2015; Saarimäki-Vire et al., 2017). Observational studies have nominated a role for STAT3 in even more cell types; profiling peripheral blood in subjects with T1D has demonstrated changes in STAT3-dependent pathways, including increased Th17 and T follicular helper cells, in new-onset T1D (Marwaha et al., 2010; Viisanen et al., 2017), and IL-6–induced phosphorylation of STAT3 is significantly increased in CD4^{+} and CD8^{+} T cells of patients with T1D (Hundhausen et al., 2016). Additional studies of human diabetogenic STAT3-GOF mutations in a physiological context are needed to resolve these results and establish the molecular and cellular links between STAT3-GOF mutations and T1D pathogenesis in vivo.

In this report, we generated STAT3 knock-in mice (STAT3[+/K392R]) carrying a single copy of the highly activating and diabetogenic missense mutation resulting in a substitution of arginine for lysine at amino acid 392 in the STAT3 DNA binding domain (K392R), which was associated with neonatal T1D in an infant at birth (Flanagan et al., 2014; Milner et al., 2015). Using this novel Mendelian mouse model, we performed a battery of phenotypic, biochemical, and functional analyses of the human STAT3-GOF mutation. Adoptive cell transfers and mouse genetic studies demonstrated a role for the mutation within the hematopoietic system and specifically within CD8^{+} T cells. We found that the mutation induces an unbridled diabetogenic CD8^{+} T cell response, which we characterize using single-cell transcriptomic, epigenetic, and T cell repertoire profiling. We determined that while CD8^{+} T cell function within the islets is typically restrained by T cell exhaustion, STAT3[+/K392R] CD8^{+} T cells are resistant to terminal exhaustion and are maintained in a highly cytotoxic state. We show that STAT3-GOF only within CD8^{+} T cells is sufficient to accelerate T1D in vivo, thus demonstrating a cell-intrinsic role for the K392R mutation in CD8^{+} T cells and establishing a defect in CD8^{+} T cell exhaustion as a contributor to T1D development.

Results and discussion
Generation of a murine model of the human STAT3 K392R mutation
To investigate the role of STAT3 hyperactivity in T1D, we took advantage of CRISPR/Cas9 editing to engineer a novel knock-in mouse on the nonobese diabetic (NOD) background incorporating the highly diabetogenic GOF human mutation (K392R) in the STAT3 gene (Fig. 1 A). To confirm that the STAT3-activating behavior of this mutation is conserved in mice, naive CD4^{+} T cells were isolated from lymphoid organs and differentiated in vitro into Th17 and T reg subsets. The STAT3[+/K392R] T cells exhibited increased differentiation of Th17 cells relative to the WT T cells, while differentiation into T reg cells was reduced (Fig. 1 B), which is consistent with GOF behavior as previously described in humans (Durant et al., 2010; Wienke et al., 2015).

Heterozygous K392R mice recapitulate the human autoimmune diabetes phenotype
We then assessed whether STAT3[+/K392R] mice exhibited the severe diabetes phenotype observed in humans. Both male and female STAT3[+/K392R] mice developed diabetes more rapidly and
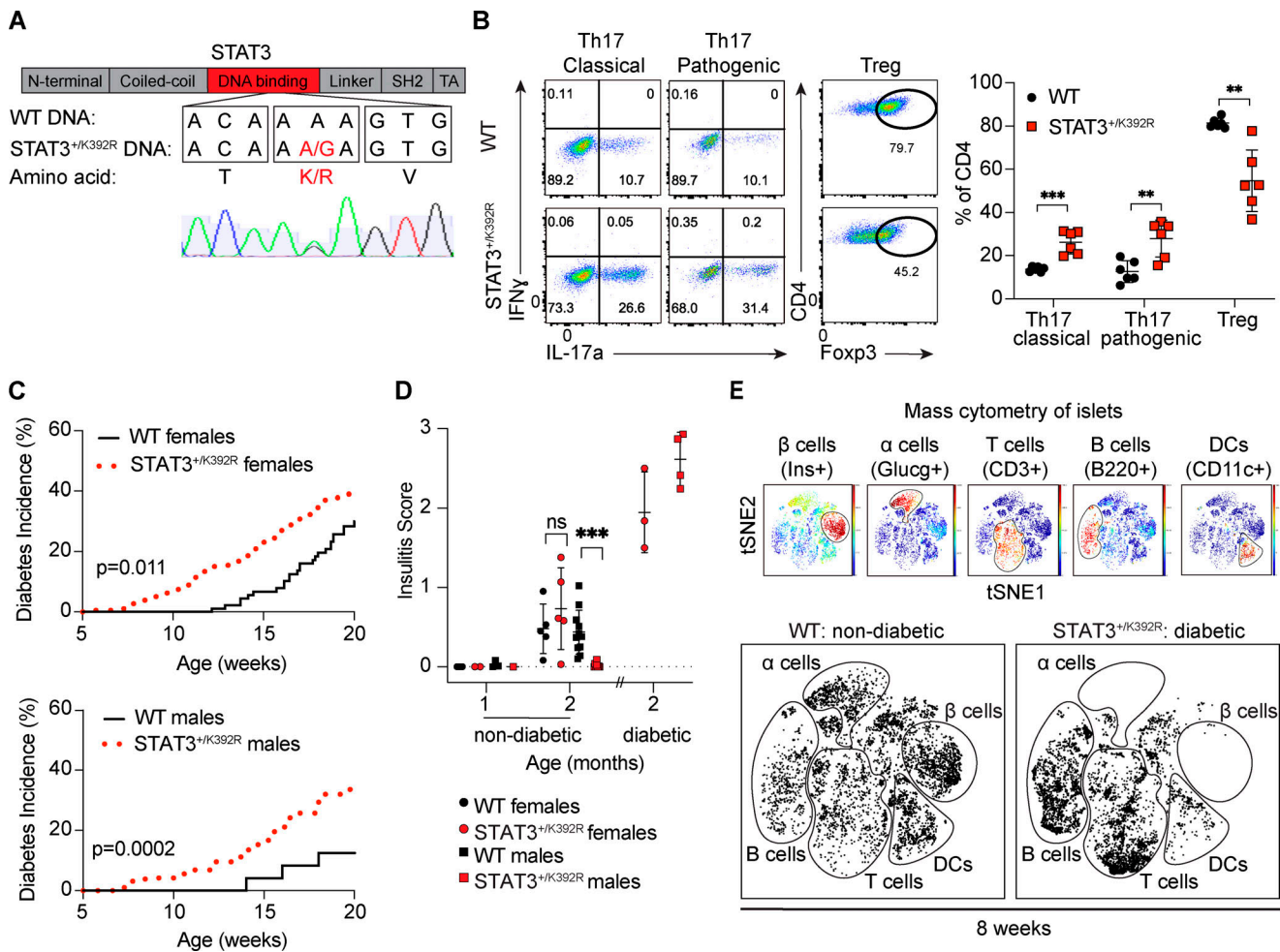
with higher incidence than their WT siblings in both sexes (Fig. 1 C). To control for potential off-target effects of gene editing, we used two independent founder lines and confirmed this diabetic phenotype in the other founder line as well (data not shown); therefore, we selected one founder line to conduct subsequent experiments. Young nondiabetic mice showed normal β cell function during glucose tolerance testing (Fig. S1 A), and immunofluorescence of STAT3[+/K392R] islets showed a normal distribution of α and β cells within the islets (Fig. S1 B), suggesting the K392R mutation did not interfere with β cell development or function as previously suggested (Saarimäki-Vire et al., 2017). Rather, diabetes onset coincided with the presence of insulin autoantibodies (Fig. S1 C) and insulitis (Fig. 1 D and Fig. S1 D) with a rapid infiltration of B and T cells at disease onset (Fig. 1 E), supporting this mouse model's recapitulation of the autoimmune diabetes phenotype observed in human patients (Flanagan et al., 2014; Milner et al., 2015).

Effector T (Teff) cells drive STAT3-GOF autoimmune diabetes
To understand the cellular compartment driving the observed autoimmunity, immunophenotyping, genetic crosses, and adoptive transfer experiments were performed. Given the time course of insulitis development and diabetes incidence (Fig. 1, C and D), we selected 6–10 wk as the age for studying the onset of autoimmunity in peripheral lymphoid tissues and within the islets. We observed lymphoproliferation grossly by increased lymphoid organ size (Fig. S1 E) and absolute lymphocyte cell counts within these organs of mice 6–8 wk of age (Fig. S1 F). Immunophenotyping of peripheral lymphocytes ex vivo by flow cytometry showed that STAT3[+/K392R] was associated with a small increase in Th17 cells but a more marked increase in Th1 cells and an increase in T reg cells (Fig. 2 A). In addition, STAT3[+/K392R] mice had expansions of their CD8^{+} effector memory and CD4^{+} memory cellular compartments (Fig. 2 A).

Given the expansion of the T cell compartment, we asked whether the adaptive immune compartment was necessary to induce diabetes by crossing STAT3[+/K392R] mice to immunodeficient NOD.Rag1^{−/−} mice, which lack mature B and T cells. STAT3[+/K392R] RAG1^{−/−} mice were completely protected from diabetes (Fig. 2 B) and had no insulitis, which confirmed the dependence on T and/or B cells in driving this disease. To further refine which compartment was essential in diabetes development, we investigated the role of the MHC in the model. Similar to the HLA haplotype DR3/4, which confers the majority of T1D risk in humans, WT NOD mice have the high-risk MHC haplotype H2[g7], which is essential for diabetes development. Thus, to determine whether STAT3[+/K392R] diabetes was MHC dependent, STAT3[+/K392R] mice were crossed to the NOD.H-2[b] strain, which carries an alternate MHC haplotype known to be protective against diabetes. NOD.H-2[b] STAT3[+/K392R] mice were completely protected from diabetes (Fig. 2 B) and had no insulitis upon histological examination (data not shown), showing that diabetes in STAT3[+/K392R] mice was an MHC-dependent disease.

The MHC dependence suggested that diabetes in STAT3[+/K392R] mice was mediated through changes either in the MHC-dependent antigen expression in target pancreatic tissue or

Warshauer et al.
STAT3-GOF disrupts CD8 tolerance to promote T1D

Journal of Experimental Medicine   2 of 15
https://doi.org/10.1084/jem.20210759

Figure 1. **STAT3^{+/K392R} mutant mice recapitulate the human T1D phenotype. (A)** STAT3^{K392R} mutation located in the DNA binding domain was inserted into WT (i.e., NOD) mice using CRISPR/Cas9 and confirmed by Sanger sequencing. TA, transactivation domain. **(B)** Naive T cells from WT and STAT3^{+/K392R} mice were differentiated in vitro under Th17 and T reg cell conditions and analyzed for intracellular cytokine or Foxp3 expression. **(C)** Diabetes onset and incidence were monitored in WT and STAT3^{+/K392R} mice up to 20 wk of age (females: WT, $n = 93$; STAT3^{+/K392R}, $n = 125$; males: WT, $n = 19$; STAT3^{+/K392R}, $n = 68$). **(D)** Time course of insulitis in WT and STAT3^{+/K392R} mice with and without diabetes ($n = 3$–11 mice per gender per time point). **(E)** viSNE plots of islets using mass cytometry to compare immune and endocrine cellular compositions between a WT mouse without diabetes and a littermate STAT3^{+/K392R} mouse with recently diagnosed diabetes to highlight the presence of immune infiltration with STAT3^{+/K392R} diabetes. Results are representative of viSNE plots from 8–14-wk-old nondiabetic WT ($n = 6$) and diabetic STAT3^{+/K392R} ($n = 4$) mice. Data in B are pooled from two independent experiments with three mice per group. A log-rank (Mantel-Cox) test (C) or Student's t test (B and D) was used. Data are shown as mean ± SD. **, $P \leq 0.01$; ***, $P \leq 0.001$.

in the MHC-mediated activation of T cells involved in β cell destruction. To establish whether the key driver of T1D was in the T cell compartment or the tissue itself, bone marrow chimeras were generated by adoptively transferring WT or STAT3^{+/K392R} bone marrow into lethally irradiated WT mice. STAT3^{+/K392R} bone marrow resulted in accelerated diabetes compared with WT bone marrow (Fig. 2 C). This result combined with the MHC dependence showed that STAT3^{+/K392R} induced autoimmune diabetes via a T cell–mediated mechanism.

Previous work in human subjects with STAT3-GOF disease has suggested dysfunctional T reg cells as a potential cause of autoimmunity (Milner et al., 2015). Therefore, we next assessed the suppressive activity of STAT3^{+/K392R} T reg cells in vivo. Adoptive transfer of islet antigen–specific T reg cells from BDC2.5 mice, which carry a CD4-specific TCR transgene that targets a pancreatic antigen derived from chromogranin A, is

effective at preventing T1D in the NOD mouse model (Stadinski et al., 2010; Tang et al., 2004; Tarbell et al., 2004), and we used this model of T reg cell suppression by crossing BDC2.5 mice to the STAT3^{+/K392R} line. To specifically examine the role of the STAT3 mutation in T reg cells, we performed adoptive transfer of naive WT BDC2.5^+ T cells into immunodeficient Rag1^{−/−} mice. This resulted in rapid development of diabetes that was ameliorated by both WT BDC2.5^+ and STAT3^{+/K392R} BDC2.5^+ T reg cells (Fig. S1 G). Therefore, STAT3^{+/K392R} did not significantly impair T reg cell function, which implicated Teff cells as key drivers of diabetes development due to the STAT3^{+/K392R} mutation.

T cell expansion is not due to priming by STAT3^{+/K392R} APCs
We next investigated whether the observed Teff cell expansion may be cell intrinsic or due to improved T cell priming by STAT3^{+/K392R} in APCs and/or the local islet environment. We
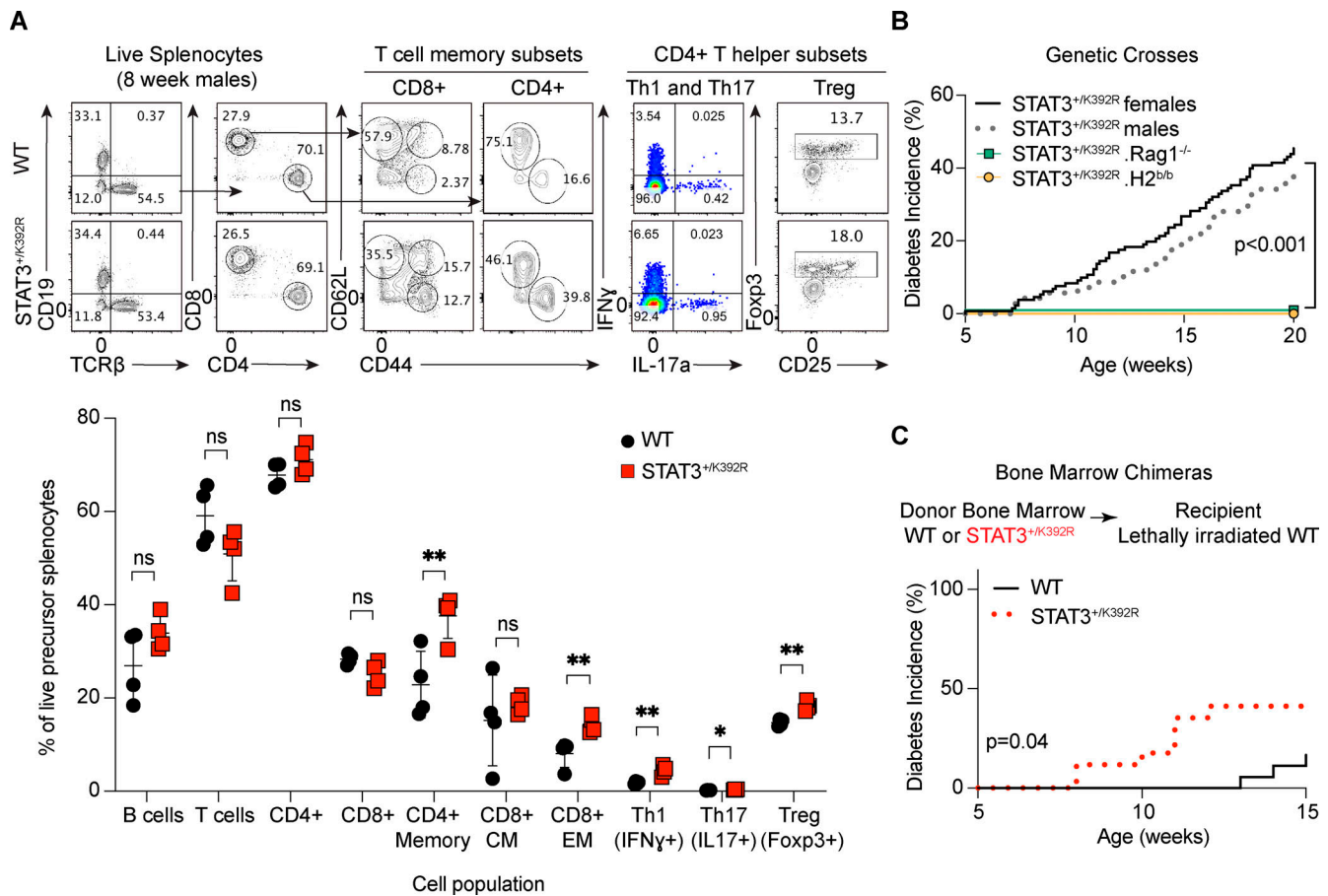
Warshauer et al.
STAT3-GOF disrupts CD8 tolerance to promote T1D

Journal of Experimental Medicine 3 of 15
https://doi.org/10.1084/jem.20210759

Figure 2. STAT3[+/K392R] Teff cell compartment. (A) Immunophenotyping of splenocytes ex vivo in 8-wk-old male mice (n = 4 per group). **(B)** Diabetes incidence in STAT3[+/K392R] RAG1^{−/−} mice (B and T cell dependence) and STAT3[+/K392R] H2[b/b] mice (MHC dependence; STAT3[+/K392R] females, n = 132; STAT3[+/K392R] males, n = 70; STAT3[+/K392R] RAG1^{−/−}, n = 9; STAT3[+/K392R] H2[b/b], n = 20). **(C)** Experimental design and subsequent diabetes incidence in bone marrow chimeras: lethally irradiated WT recipients adoptively transferred with bone marrow from WT (n = 18) or STAT3[+/K392R] (n = 17) mice. Data in A are representative of two independent experiments with three or four mice per group. Student's t test (A), Mantel-Cox log-rank test (B), or Gehan-Breslow-Wilcoxon test (C) was used. Data are shown as mean ± SD. *, P ≤ 0.05; **, P ≤ 0.01. CM, central memory; EM, effector memory.

performed ex vivo immunophenotyping by flow cytometry of 8-wk-old nondiabetic STAT3[+/K392R] APCs within the spleen and found that STAT3[+/K392R] did not significantly alter population frequencies of monocytes, pre-dendritic cells (pre-DCs), or DCs (Fig. 3 A). We next immunophenotyped APCs directly within the islets using mass cytometry and observed that the expression of classical molecules needed for antigen presentation to T cells, MHC class II and CD86, also appeared undisturbed in 8–10-wk-old nondiabetic mice (Fig. 3 B). We then performed transcriptional profiling of the infiltrating immune cells using single-cell RNA sequencing (scRNA-seq) of CD45^{+} lymphocytes isolated from islets of 8–10-wk-old nondiabetic mice. We obtained high-quality scRNA profiles for 20,361 high-quality single cells from STAT3[+/K392R] and WT mice. Cells were clustered and then visualized using Seurat (Fig. S2 A), followed by a reclustering of only the CD11c^{+} APCs (Fig. 3 C) for further analysis. Expression of canonical immune cell markers was computed and used to uniquely identify the six cell populations represented by each cluster, which included conventional DCs, plasmacytoid DCs, macrophages, and monocytes (Fig. S2 B). Overall, cluster population frequencies were similar between STAT3[+/K392R] and

WT cells (Fig. 3 D), consistent with our flow cytometry data (Fig. 3 A). Corroborating our mass cytometry data (Fig. 3 B), expression of antigen-presenting genes Cd86 and MHC-II (H2-Ab1) appeared comparable (Fig. 3 E) among the different APC populations. Altogether, these results supported phenotypic similarity between STAT3[+/K392R] and WT APCs.

Finally, we performed a functional experiment to test whether STAT3[+/K392R] in APCs and/or the local islet environment was priming T cells and driving their increased proliferation. Naive CD4^{+} BDC2.5Tg^{+} cells were isolated by FACS from nondiabetic BDC2.5Tg^{+} donors, labeled with CellTrace Violet (CTV) to track cellular activation and proliferation, and adoptively transferred into STAT3[+/K392R] or WT hosts. Proliferation was evaluated 3.5 d after cell transfer by FACS analysis of the CTV dye dilution in the pancreatic LNs (pLNs) and inguinal LNs (LNs; control) of recipient mice, and there was no evidence to support the local islet environment as a driver of T cell priming and activation (Fig. 3 F). Overall, the lack of evidence to support an effect of STAT3[+/K392R] on the APC compartment suggested that the diabetogenic effect of STAT3[+/K392R] was intrinsic to the Teff cells rather than their surrounding environment.
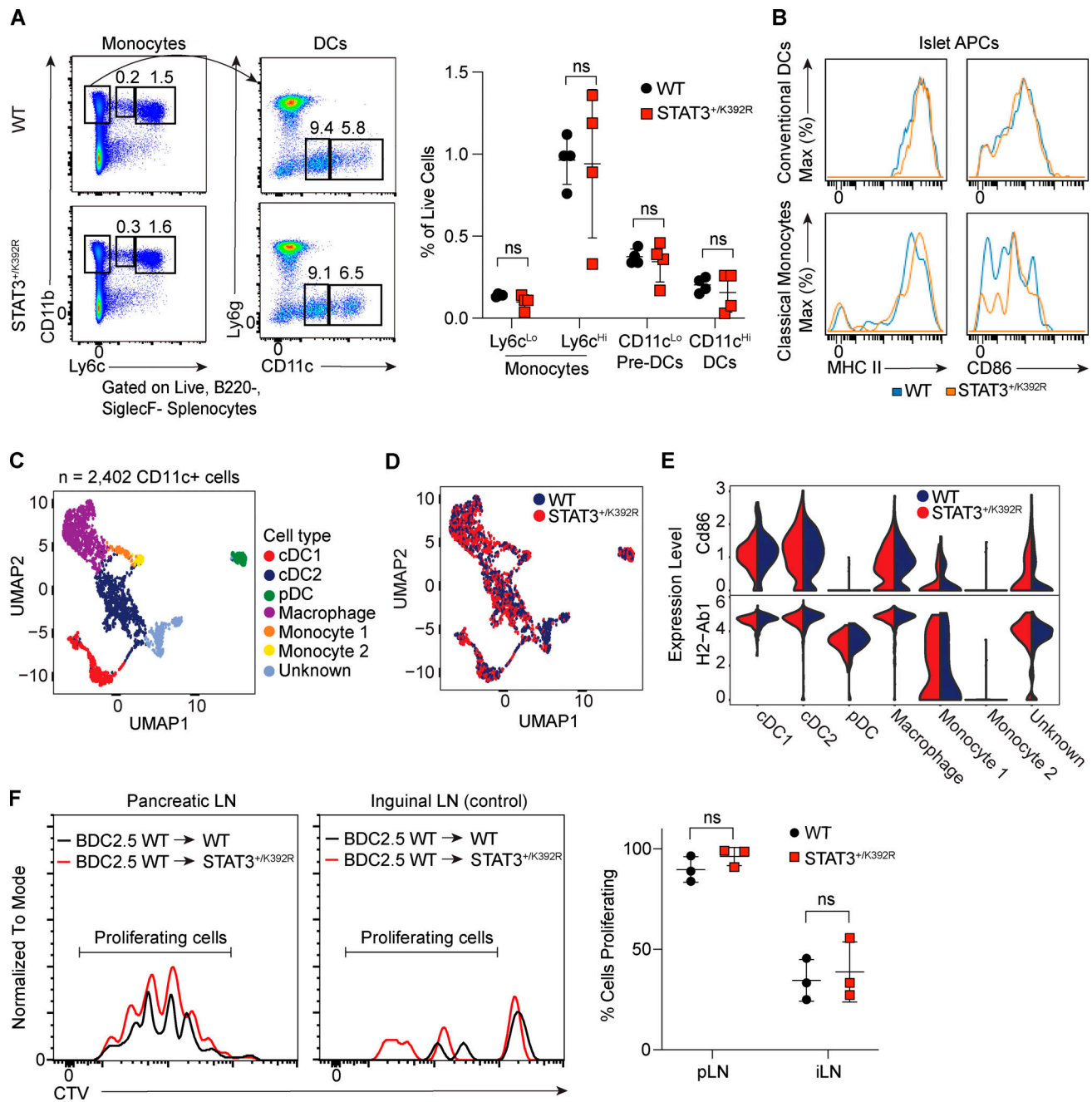
Figure 3. **STAT3[+/K392R] APC phenotype and T cell priming by the local islet environment is unchanged. (A)** Flow cytometry gating (values shown are frequency relative to parent gate) and population frequencies of APC subpopulations from splenocytes isolated ex vivo in nondiabetic 8-wk-old male mice (*n* = 4 per group). **(B)** Representative histograms for MHC II and CD86 protein expression on conventional DCs (CD11c^{+}MHC II^{+}) and classical monocytes (CD11b^{+}Ly6c^{+}) in the islets of nondiabetic 8–10-wk-old mice using mass cytometry. **(C)** Uniform Manifold Approximation and Projection for Dimension Reduction (UMAP) projection of reclustered antigen-presenting myeloid cells (CD11c^{+} cells) from islet immune infiltrates of 8–10-wk-old nondiabetic WT (*n* = 3, pooled) and STAT3[+/K392R] (*n* = 3, pooled) mice used in scRNA-seq experiment (see Fig. S1). **(D)** UMAP projection showing distribution of STAT3[+/K392R] and WT cell transcriptomes. **(E)** Violin plots showing gene expression profile of *MHCII* and *CD86* in APC myeloid clusters. **(F)** Representative CTV profiles (left) of BDC2.5 CD4^{+} T cells in pLNs and iLNs (control) 3.5 d after adoptive transfer into STAT3[+/K392R] and WT recipients. Cell proliferation was evaluated by FACS analysis of the CTV dilution in the pLNs and iLNs of recipient mice (*n* = 3 per group), and results are expressed as the percentage of proliferating cells within the recovered CTV-labeled BDC2.5 CD4^{+} T cells (right). Data are representative of two independent experiments (A and F) or three sets of littermates (B). Student's *t* test (A and F) was used. Data are shown as mean ± SD.

STAT3-GOF up-regulates chemotactic and cytotoxic gene expression in CD8^{+} T cells

To better understand the molecular mechanisms of STAT3[+/-K392R] within Teff cells, we performed paired transcriptomic and

TCR sequencing (TCR-seq) in single cells (scRNA-seq/TCR-seq) from CD45^{+} lymphocytes isolated from islets of the 8–10-wk-old nondiabetic mice used in the earlier scRNA-seq experiment (Fig. S2 A). A total of 8,725 CD3^{+} T cells were reclustered and used for

Warshauer et al.
STAT3-GOF disrupts CD8 tolerance to promote T1D

Journal of Experimental Medicine   5 of 15
https://doi.org/10.1084/jem.20210759

further analysis (Fig. 4 A). Differentially expressed marker genes for each cluster were computed (Fig. S2 C) along with canonical marker gene expression (Fig. S2, D and E) and used to uniquely identify the cell populations represented by each T cell cluster. Comparisons of the STAT3$^{+/K392R}$ versus WT clusters showed a marked expansion of effector CD8$^+$ T cells and a corresponding decrease in naive CD8$^+$ T cells (Fig. 4 A). Notably, no increase in T reg or Th17 cell populations in these islet infiltrates was observed. Differential gene expression comparing the STAT3$^{+/K392R}$ versus WT CD8$^+$ T cells showed that STAT3$^{+/K392R}$ drove a highly cytotoxic CD8$^+$ T cell phenotype with up-regulation of genes involved in chemotaxis (e.g., *Ccl4* and *Ccl5*) and cytotoxicity (e.g., *Gzma*, *Gzmb*, *Gzmk*; Fig. 4 B). To confirm these findings at the protein level, we performed flow cytometry and found that STAT3$^{+/K392R}$ CD8$^+$ T cells isolated from the pLN showed increased Ccl5 expression relative to WT (Fig. 4 C) and that CD8$^+$ T cells from the spleen showed increased granzyme A and granzyme B protein expression (Fig. S2 F).

To provide deeper characterization of the expanded STAT3$^{+/K392R}$ CD8$^+$ T cells, a total of 2,034 CD8$^+$ T cells were reclustered for further analysis (Fig. 4 D). We identified clustered cell populations by their expression of canonical CD8 markers (Fig. 4 E), in addition to using module scores to distinguish terminally exhausted T cells (*Cd101*, *Cd200r2*, *Cd7*, *Cd200r1*, *Il10*) and transitory T cells (*Cx3cr1*, *Klrg1*, *Il2ra*, *Il18rap*, *S1pr5*; Fig. 4 F), as previously described (Hudson et al., 2019). Focusing on the expanded nonnaive cell populations, STAT3$^{+/K392R}$ cells exhibited a bias toward the transitory (versus terminally) exhausted CD8$^+$ T cell phenotype (Fig. 4 G) with a STAT3$^{+/K392R}$ transitory/terminally exhausted ratio 2.5 times that of WT. The gene signatures of the effector and transitory clusters (Fig. 4 H) closely matched that of the differential gene expression seen across CD8 T cells in aggregate (Fig. 4 B), which suggested that the phenotypic difference in CD8 T cells caused by STAT3$^{+/K392R}$ was driven by an increased proportion of transitory cells with a cytotoxic gene expression profile, while WT cells preferentially exhibited a terminally exhausted phenotype.

STAT3-GOF epigenetically regulates chemotactic and cytotoxic genes in effector CD8$^+$ T cells

In parallel to our single-cell transcriptomic approach, we also used single-cell epigenetics to examine the chromatin state in infiltrating immune cells in the islets. We performed single-cell ATAC sequencing (scATAC-seq) on CD45$^+$ infiltrating islet cells of 8–10-wk-old nondiabetic mice such as those used in the scRNA-seq studies and obtained high-quality ATAC-seq profiles from 17,466 single cells with a median number of 5,610 fragments per cell and a median enrichment of Tn5 insertions in transcription start sites for 17.11. To identify cell types and determine a correspondence between the scRNA-seq clusters and the scATAC-seq clusters, we used gene scores, which are computed by aggregating the ATAC-seq signal across the gene body and promoter in each cell (Fig. S3 A). By analyzing the corresponding clusters, we were able to link our gene expression findings with epigenetic changes in the same cell types. There were 197 peaks with significantly increased chromatin

accessibility whose nearest gene was 1 of the 129 significantly up-regulated genes (log fold change, ≥0.25; and padj ≤ 0.05; Fig. S3, B and C). Key molecules characteristic of cytotoxic CD8$^+$ T cells, including *Ccl5*, *Klrg1*, and *Gzma*, had multiple nearby significant peaks (Fig. S3 B), indicating epigenetic regulation of the Teff cell gene expression program induced in STAT3$^{+/K392R}$ compared with WT mice. We next sought to determine which transcription factors might be responsible for the observed epigenetic remodeling in the CD8$^+$ T cell compartment. Comparing transcription factor motif accessibility between STAT3$^{+/K392R}$ and WT CD8$^+$ T cells using chromVAR (Schep et al., 2017) identified 406 motifs with significantly different activity (false discovery rate, ≤0.1; |mean difference| ≥ 0.01). Eomesodermin (Eomes) and Tbx21 were among the significantly more accessible transcription factors, and they have well-established roles in Teff cell development and function (Kaech and Cui, 2012; Fig. S3, D and E). Transcription factors involved in programming tissue residency in CD8$^+$ T cells were among the most significantly different, in particular the increased accessibility of Runx3 (Milner et al., 2017) and decreased accessibility of Klf2 (Weinreich et al., 2009; Fig. S3, D and E). In sum, STAT3$^{+/K392R}$ leads to increased activity of transcription factors involved in tissue infiltration and cytotoxic gene expression programs in CD8$^+$ Teff cells.

STAT3-GOF in diabetogenic CD8$^+$ T cells is sufficient to accelerate T1D

Finally, we sought to establish whether these STAT3$^{+/K392R}$ effector CD8$^+$ T cells were directly responsible for the autoimmune diabetic phenotype. We analyzed the TCR repertoire data obtained from the scRNA-seq/TCR-seq experiment to characterize the specificity of the infiltrating CD8$^+$ T cells and determine whether they were indeed directly diabetogenic. We recovered high-confidence TCR sequences for 91% of T cells (Fig. S3 F). We used the Gini index to quantify the extent of TCR clonal expansion within each cluster and found that the STAT3$^{+/K392R}$ effector CD8$^+$ T cell cluster exhibited increased clonal expansion relative to WT (Fig. S3 G), suggesting that these cells were recognizing and proliferating in response to islet antigens. We then analyzed the top 20 most abundant CD8$^+$ TCR clones and identified clone 6158, which was present in both STAT3$^{+/K392R}$ and WT mice (Fig. 5 A). This specific clone contained CDR3 sequences nearly identical to those found in the TCR-8.3 (Fig. 5 B), a CD8-restricted TCR specific for the islet-specific glucose 6-phosphatase–related protein (IGRP) antigen that is known to be diabetogenic in NOD mice (8.3Tg$^+$; Verdaguer et al., 1997). Because this clone was shared between the two genotypes, we crossed the 8.3Tg$^+$ mouse with the STAT3$^{+/K392R}$ line and assessed diabetes incidence to isolate whether the underlying transcriptional and epigenetic changes were key drivers underlying the STAT3$^{+/K392R}$ diabetogenic effect. Consistent with a STAT3-GOF–intrinsic effect on CD8$^+$ T cells, STAT3$^{+/K392R}$ 8.3Tg$^+$ mice became rapidly diabetic and with a much higher diabetes incidence than WT 8.3Tg$^+$ mice (Fig. 5 C).

To then test whether STAT3-GOF in diabetogenic CD8$^+$ T cells was sufficient to accelerate T1D, we used an established adoptive transfer model in which polyclonal CD4$^+$ T cells are transferred

Warshauer et al.
STAT3-GOF disrupts CD8 tolerance to promote T1D

Journal of Experimental Medicine   6 of 15
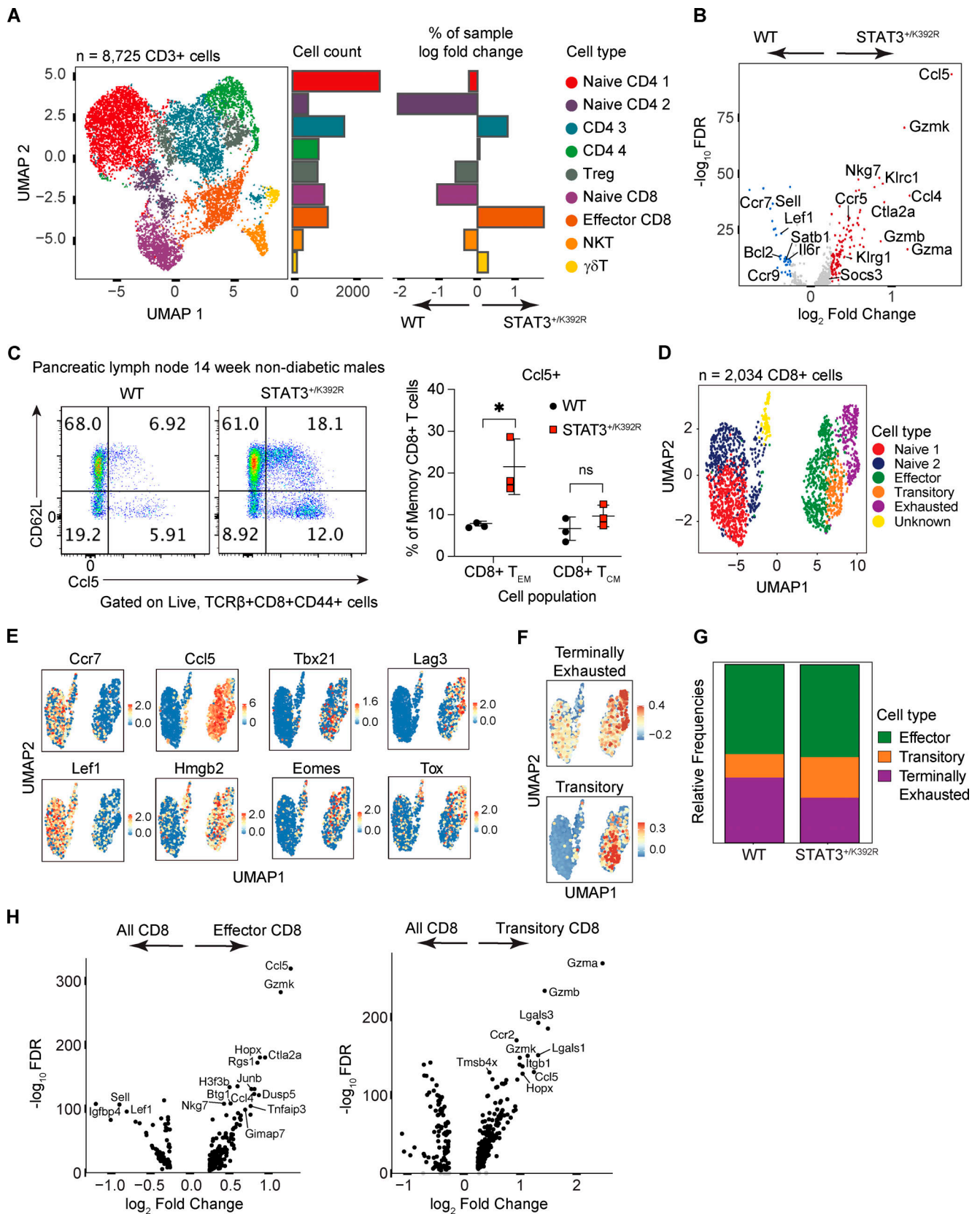https://doi.org/10.1084/jem.20210759

Figure 4. **STAT3^{+/K392R} drives expansion of the CD8+ effector compartment with up-regulation of cytokine and chemokine genes. (A)** UMAP projection of reclustered T cells (CD3+ cells) from islet immune infiltrate used in scRNA-seq experiment (see Fig. S2 A) with associated cell counts per cluster and comparison of cluster frequencies between the two genotypes (STAT3^{+/K392R} versus WT). γδT, γδ T cells. **(B)** Volcano plot showing STAT3^{+/K392R} versus WT differential gene expression in CD8+ clusters. FDR, false discovery rate. **(C)** Flow cytometry of Ccl5 protein expression in CD8+ memory T cells from the pLN in

Warshauer et al.
STAT3-GOF disrupts CD8 tolerance to promote T1D

Journal of Experimental Medicine
https://doi.org/10.1084/jem.20210759

nondiabetic males at 14 wk (*n* = 3 per group). **(D)** UMAP projection of reclustered CD8^{+} T cells. **(E and F)** Marker gene (E) or module score (F) expression in CD8^{+} T cell clusters. In F, genes used to calculate module scores for terminally exhausted T cells were *Cd101, Cd200r2, Cd7, Cd200r1,* and *Il10,* and for transitory T cells, they were *Cx3cr1, Klrg1, Il2ra, Il18rap,* and *S1pr5,* as previously described (Hudson et al., 2019). **(G)** Relative population frequencies among nonnaive CD8^{+} cell clusters. **(H)** Volcano plot showing differential gene expression in CD8^{+} effector and transitory cell clusters relative to all CD8^{+} cells. Differential gene expression (B and H) based on nonparametric Wilcoxon rank-sum test. Volcano plots (B and H) use log *N* fold cutoff 0.25, and genes of interest are labeled. Data in C are representative of two independent experiments. Student's *t* test (C) was used. Data are shown as mean ± SD. *, P ≤ 0.05.

with naive 8.3-TCR transgenic CD8^{+} T cells and start inducing diabetes within 1 mo of transfer into NOD.SCID recipients (Christianson et al., 1993; De Leenheer and Wong, 2015; Jun et al., 1999). NOD.SCID mice adoptively transferred with polyclonal WT CD4^{+} T cells and naive CD8^{+} T cells from STAT3[+/K392R] 8.3Tg^{+} mice experienced significantly accelerated diabetes onset compared with mice that instead received their naive CD8^{+} T cells from WT 8.3Tg^{+} mice (Fig. 5 D). Because no other immune populations were present in the recipient NOD.SCID mice, this experiment established that STAT3-GOF in diabetogenic CD8^{+} T cells is sufficient to drive the autoimmune diabetic phenotype. We also performed adoptive transfer experiments to

understand whether CD4^{+} cells might also be playing a key role in STAT3-GOF diabetes and did not find evidence to support this. First, naive CD8^{+} cells from WT 8.3Tg^{+} mice transferred with polyclonal CD4^{+} cells from either STAT3[+/K392R] or WT mice into NOD.SCID mice did not cause a noticeable difference in diabetes incidence, which suggested that the diabetogenic effect of STAT3[+/K392R] was likely intrinsic to its role in CD8^{+} T cells rather than an indirect result of CD4 help to the CD8^{+} population (Fig. S3 H). Second, the adoptive transfer of either WT BDC2.5^{+} or STAT3[+/K392R] BDC2.5^{+} CD4^{+} Teff cells into NOD.Rag1^{−/−} mice did not result in differing diabetes incidences, suggesting that CD4^{+} cells alone were insufficient drivers of the accelerated
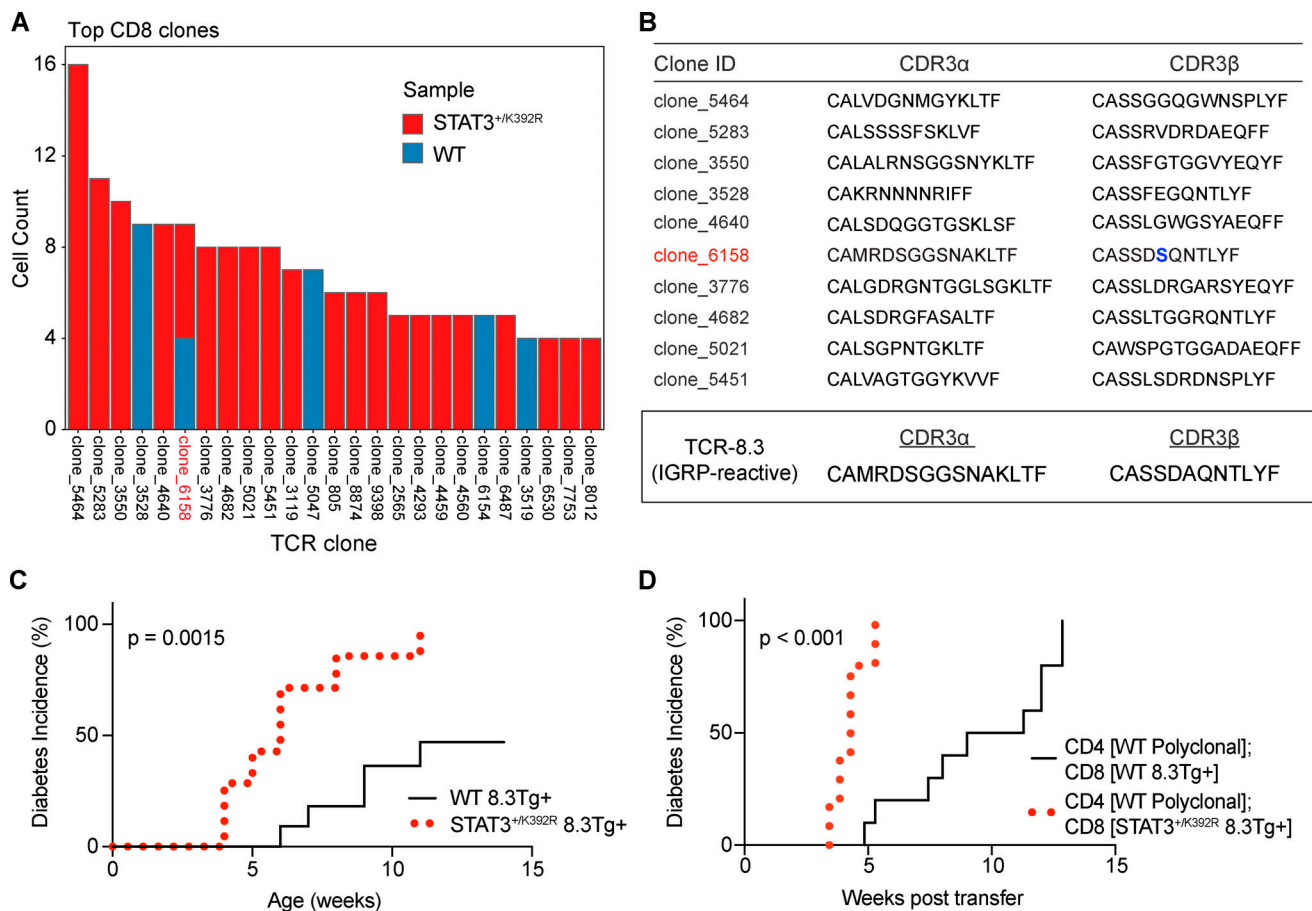

Figure 5. **STAT3[+/K392R] drives clonal expansion of diabetogenic CD8^{+} T cells. (A)** Top 20 CD8 clones by count in each sample. **(B)** Top 10 specific CD8 clones with corresponding CDR3 sequences displayed. The CDR3 sequence for clone 6158 in red is nearly identical to that of the CD8-restricted TCR specific for islet-specific antigen IGRP (TCR-8.3; sequence shown below table). The only difference between clone 6158 and TCR-8.3 is a serine, denoted in blue, that replaces an alanine of the TCR-β chain. **(C)** Diabetes incidence of 8.3Tg[+] (IGRP-specific TCR) mice with (*n* = 7) and without (*n* = 11) STAT3[+/K392R] confirms increased diabetogenicity. **(D)** Diabetes incidence after adoptive transfer of polyclonal WT CD4^{+} T cells with naive CD8^{+} T cells from 8.3Tg^{+} mice with (*n* = 5) and without STAT3[+/K392R] (*n* = 10) into NOD.SCID mice. Results are pooled from two independent experiments. A log-rank (Mantel-Cox) test (C and D) was used.

diabetic phenotype (Fig. S3 H). Altogether, these findings showed that effector CD8+ cells were the key drivers of STAT3-GOF diabetes, and in combination with our molecular data, they established a direct mechanism used by STAT3 to promote T1D through a defect in CD8+ T cell tolerance.

In sum, we generated a novel Mendelian model of monogenic autoimmune diabetes based on a human STAT3-GOF mutation, identified how it caused an unbridled autoreactive effector CD8+ T cell response at the epigenetic and transcriptomic levels, and confirmed that these findings are sufficient to accelerate T1D in vivo, thus establishing a novel direct pathway involved in T1D pathogenesis. Our findings are surprising, given prior assumptions from ex vivo and in vitro studies in which STAT3-GOF caused T1D via Th17/T reg cell imbalance (Fabbri et al., 2019; Milner et al., 2015) or an islet-intrinsic defect (Saarimäki-Vire et al., 2017), and highlight the value of in vivo study of human mutations to uncover mechanisms underlying diseases. However, our findings are also consistent with STAT3's known role in driving formation of memory CD8+ T cells (Cui et al., 2011), which have a highly proliferative potential and long-term survival, consistent with the CD8+ T cell expansions we observed in our STAT3-GOF mouse model in the secondary lymphoid organs and islets. STAT3 is required to sustain the expression of EOMES (Ciucci et al., 2017), another key transcription factor involved in the effector cell–memory cell transition and that we observed had more motif activity in our ATAC-seq data. Because the mutation we studied is in the DNA binding domain, we speculate that STAT3-GOF is inducing an opening of chromatin regions within activated CD8+ T cells that are associated with chemotaxis (e.g., Ccl4 and Ccl5), cytotoxicity (e.g., Gzma, Gzmb, Gzmk), and memory homeostasis (e.g., Tbx21 and Eomes), which leads to a more diabetogenic CD8+ T cell population. Cytotoxic CD8+ T cells exhibiting up-regulation of genes we identified have been observed within islets of NOD mice by others but appear to be more restrained under normal STAT3 activity (Zakharov et al., 2020), and our results provide further insight into the epigenetic and transcriptomic mechanisms that allow β cell–specific CD8+ T cell responses to remain long-lived (Abdelsamed et al., 2020) by demonstrating a key regulatory role of STAT3. In addition to DNA binding domain mutations contributing to T1D, diabetogenic STAT3-GOF mutations have also been reported in the coiled-coil (Maffucci et al., 2016; Milner et al., 2015), transactivation (Flanagan et al., 2014; Nabhani et al., 2017; Sediva et al., 2017), and SH2 (Flanagan et al., 2014) domains. Future investigations are needed to see whether other mechanisms are at play for mutations that occur at sites outside the DNA binding domain, because each domain carries a distinct functional role: The coiled-coil domain mediates cytokine receptor interaction and subsequent phosphorylation; the DNA binding domain increases DNA binding capacity that leads to enhanced transcriptional activity; the transactivation domain mediates transcriptional activation and recruitment of cotranscriptional factors; and the SH2 domain supports DNA binding affinity via electrostatic interactions with the DNA backbone (Fabbri et al., 2019; Faletti et al., 2021).

Our findings suggest that STAT3+/K392R causes excessive CD8 T cell effector activity by impeding the development of terminal exhaustion and instead retaining CD8 effector cells in a highly cytotoxic (and typically transitory) phenotype. It has been shown CD8 exhaustion follows a spectrum (Beltra et al., 2020), with different exhausted CD8 T cell subsets retaining different levels of effector functions (Im et al., 2016; Siddiqui et al., 2019; Wu et al., 2016). The transitory CD8 population, similar to Texint previously described (Beltra et al., 2020), carries more proliferative capacity and effector-like function (e.g., up-regulation of genes such as Tbx21 and Gzmb) than terminally exhausted CD8 cells that are less functional (Hudson et al., 2019). This aligns with our findings of an expanded CD8 T cell compartment containing a similar cytotoxic profile and that subsequently induces acceleration of diabetes onset. The transitory population also expands in response to PD-1 pathway blockade and is thought to play a critical role in therapeutic response to checkpoint blockade used in cancer immunotherapy (Beltra et al., 2020; Hudson et al., 2019). Separately, it has been shown that T cell exhaustion is important in determining autoimmune disease outcomes (McKinney et al., 2015) and that PD-1–deficient NOD mice develop accelerated diabetes (Ansari et al., 2003; Keir et al., 2006). Our findings help bridge these important sets of knowledge by expanding the role of transitory exhausted T cells to autoimmune disease and T1D. This is consistent with recent observations in studying T1D progression in humans showing that individuals with a higher activated transitional memory CD8 phenotype tended to progress more rapidly to T1D, while individuals with a more terminally exhausted CD8 phenotype had a slower rate of T1D progression (Wiedeman et al., 2020). Our results also align with the positive associations between exhausted CD8+ T cells and T1D immunotherapy treatment response during landmark T1D prevention and reversal trials using the anti-CD3 mAb teplizumab (Herold et al., 2019; Long et al., 2016; Sims et al., 2021). This underscores how using a mouse model rooted in a human mutation can provide cellular and molecular insights into the determinants of response in human T1D clinical trials. In addition, this work may help further our understanding of how unintended autoimmune toxicities, such as T1D, result from cancer immunotherapies and how we might develop strategies to prevent them (June et al., 2017). Altogether, our new model has allowed us to determine how this transitory state may be a key tolerance pathway that keeps T1D in check.

Historically, T1D development has been studied in the context of central tolerance mechanisms (via the study of human AIRE mutations) and peripheral suppressor mechanisms (via the study of human FOXP3 mutations). Therefore, our findings fill an important void necessary for understanding this complex autoimmune disease by establishing that CD8+ T cell tolerance also plays a key role in T1D immunopathogenesis (Buckner and Nepom, 2016; Ihantola et al., 2018; Yeo et al., 2018). Our studies support an important protective role for CD8 T cell exhaustion in T1D and suggest that modulating CD8 T cell function may be a therapeutic opportunity for the prevention and treatment of human T1D.

Materials and methods

Mice

The single-nucleotide variant 1454 A>G of NM_011486.3 identified in a STAT3-GOF patient was inserted using CRISPR/Cas9

Warshauer et al.
STAT3-GOF disrupts CD8 tolerance to promote T1D

Journal of Experimental Medicine 9 of 15
https://doi.org/10.1084/jem.20210759

genome editing by The Jackson Laboratory in a custom request (Madisen et al., 2010). Two founder lines were used for experiments to minimize the risk of off-target effects. Additionally, The Jackson Laboratory provided other mice used in these experiments: NOD (Jax 001976), NOD.RAG1$^{-/-}$ (Jax 003729), NOD.SCID (Jax 001303), NOD.H2$^{b/b}$ (Jax 002591), NOD.BDC2.5$^+$ (Jax 004460), and NOD.8.3TCR$^+$ (Jax 005868; Madisen et al., 2010), unless otherwise specified in the Materials and methods section.

Mice were maintained in the University of California, San Francisco (UCSF) specific pathogen–free animal facility in accordance with the guidelines established by the Institutional Animal Care and Use Committee and Laboratory Animal Resource Center, and all experimental procedures were approved by the Laboratory Animal Resource Center at UCSF. Mice aged 4–8 wk were used for all experiments unless otherwise specified in the text or figure legends. Mice were age matched in figures displaying a single representative experiment and in pooled data.

Lymphocyte isolation, cell sorting, and flow cytometry
LNs and spleens were isolated by dissection from mice and then mashed through a 70-μm filter. Spleen cells were lysed in ammonium chloride potassium lysis buffer to remove RBCs. Cells isolated from spleens and LNs were counted, and 1–5 × 10^6 cells were first stained in PBS and Ghost Live/Dead (Tonbo Biosciences), followed by blocking in 2.4G2 before staining with the appropriate antibodies for flow cytometry. For transcription factor staining, cells were fixed overnight using the eBioscience Foxp3/Transcription Factor/Fixation-Concentrate kit (Thermo Fisher Scientific). After fixation, cells were permeabilized and stained with the appropriate antibodies. For intracellular staining, cells were stimulated for 4 h in Brefeldin A (eBioscience) and eBioscience Cell Stimulation Cocktail (500×). Cells were then fixed and permeabilized using the BD Cytofix/Cytoperm kit before being stained with the appropriate antibodies.

Islets were purified following standard collagenase protocols as described previously (Tang et al., 2004) and were dissociated by incubation with a nonenzymatic solution (Sigma-Aldrich) followed by trituration per the manufacturer's instructions.

Antibodies used for flow cytometry were as follows: PE-Cy7–conjugated B220 (clone RA3-6B2; BioLegend), peridinin-chlorophyll-protein (PerCP)-conjugated CD11b (clone M1/70; BioLegend), BV421-conjugated CD11c (clone N418; BioLegend), FITC-conjugated CD19 (clone 1D3; BD Biosciences), BV605-conjugated CD4 (clone GK1.5; BioLegend), PE-Cy7–conjugated CD4 (clone RM4-5; Tonbo Biosciences), APC-eFluor780–conjugated CD44 (clone IM7; Invitrogen), PerCP-Cy5.5–conjugated CD44 (clone IM7; Tonbo Biosciences), PE-Cy7–conjugated CD45 (clone 30-F11; Invitrogen), APC-conjugated CD62L (clone MEL-14; BioLegend), PE-Cy7–conjugated CD62L (clone MEL-14; Invitrogen), PerCP-conjugated CD8a (clone 53-6.7; BioLegend), PerCP-Cy5.5–conjugated CD8a (clone 53-6.7; BioLegend), PacOrange-conjugated CD8a (clone 5H10; Invitrogen), APC-eFluor780–conjugated CD25 (clone PC61.5; Invitrogen), FITC-conjugated FoxP3 (clone FJK-16s; Invitrogen), BV785-conjugated IFNγ (clone XMG1.2; BioLegend), FITC-conjugated IFNγ (clone XMG1.2; Tonbo Biosciences), APC-conjugated IL17a (clone eBio17B7; Invitrogen), PE-conjugated IL17a (clone eBio17B7; Invitrogen), APC-eFluor780–conjugated

Ly6c (clone HK1.4; Invitrogen), FITC-conjugated Ly6g (clone RB6-8C5; Tonbo Biosciences), PE-conjugated Siglec-F (clone E50-2440; Invitrogen), APC-eFluor780–conjugated TCRβ (clone H57-597; Invitrogen), BV421-conjugated TCRβ (clone H57-597; BioLegend), PE-conjugated Vb4 (clone KT4; BD Biosciences), PE-conjugated Ccl5 (clone 2E9; BioLegend), PE-conjugated granzyme A (clone 3G8.5; BioLegend), and Ghost UV450 (Tonbo).

Cytokine production
Lymphocytes were activated at 10^6 cells/ml with 0.5 mM ionomycin, 10 ng/ml PMA, and 3 mg/ml Brefeldin A at 37°C for 3–4 h before labeling with LIVE/DEAD fixable dead stain and staining for CD4, CD8, IL-17, and IFNγ using Cytofix/Cytoperm.

T cell differentiation
T cells were enriched from spleens and LNs using the MagniSort CD4 negative selection kit (Thermo Fisher Scientific). Naive CD4$^+$ T cells were isolated by flow cytometry on the basis of markers CD4$^+$CD62L$^+$CD44$^-$CD25$^-$ or using the EasySep mouse naive T cell isolation kit. 10^5 naive T cells were cultured for 4 d (Th17 and induced T reg [iT reg] cells) in a 96-well flat-bottom plate coated with 2 μg/ml anti-CD3 (clone 2C11; Tonbo Biosciences) and 2 μg/ml anti-CD28 (clone 37.51; Tonbo Biosciences) with the relevant cytokines and blocking antibodies: classical Th17 (20 ng/ml IL-6, 2 ng/ml TGFβ, 10 μg/ml anti-IL4 [clone 11B11; Tonbo Biosciences], and 10 μg/ml anti-IFNγ [clone XMG1.2; Tonbo Biosciences]), pathogenic Th17 (20 ng/ml IL-6, 20 ng/ml IL-1β, 20 ng/ml IL-23, 10 μg/ml anti-IL4, and 10 μg/ml anti-IFNγ), iT reg cells (20 ng/ml TGFβ and 100 U/ml IL-2), or Th0 cells (100 U/ml IL-2). Th17 cell cultures were performed in Iscove's medium, and iT reg cell cultures were performed in RPMI medium. All media were supplemented with 10% FBS, penicillin/streptomycin, glucose, pyruvate, β-mercaptoethanol, and Hepes. Cytokines were purchased from R&D Systems (murine IL-6 and human IL-2), Miltenyi Biotec (murine IL-1β and murine IL-23), or ProteinTech (HumanKine; human TGFβ).

Mass cytometry of islets
Islets were purified following standard collagenase protocols as described previously (Tang et al., 2004) and dissociated by incubating with a nonenzymatic solution (Sigma-Aldrich) followed by trituration per the manufacturer's instructions. Single-cell suspensions were fixed for 10 min at room temperature (RT) using 1.6% paraformaldehyde (Fisher Scientific). Mass-tag cellular barcoding was performed as previously described (Zunder et al., 2015), followed by sample pooling. Cells were then stained as previously reported (Levine et al., 2020). Primary conjugates of mass cytometry antibodies were prepared using the MaxPAR antibody conjugation kit (Fluidigm) according to the manufacturer's recommended protocol, and each antibody clone and lot were titrated to optimal staining concentrations using primary murine samples. Prior to sample acquisition, cells were stained with 125 nM Ir191/193 DNA intercalator (Cell-ID Intercalator-Ir; Fluidigm) for 20 min, washed in deionized water, filtered through a 35-μm nylon mesh, and resuspended to 0.5 × 10^6 cells/ml with 0.1% EQ Four Element Calibration Beads (Fluidigm). Data acquisition was carried out with a CyTOF 2 mass

Warshauer et al.
STAT3-GOF disrupts CD8 tolerance to promote T1D

Journal of Experimental Medicine   10 of 15
https://doi.org/10.1084/jem.20210759

cytometer (Fluidigm) at an event rate of 300–500 cells/s. After data acquisition, .fcs files were concatenated, normalized using mass bead signal (Finck et al., 2013), and debarcoded using a single-cell debarcoding algorithm (Zunder et al., 2015). Manual gating and visualization with t-distributed stochastic neighbor embedding (viSNE) analysis of .fcs files was performed using Cytobank (Kotecha et al., 2010).

Antibodies used for mass cytometry were as follows: [89]Y-conjugated CD45 (clone A20; BioLegend), [113]In-conjugated Ter119 (clone TER-119; BioLegend), [139]La-conjugated Ly6g (clone 1A8; UCSF), [140]Ce-conjugated KLRG1 (clone 2F1; BD Biosciences), [142]Nd-conjugated CD49b (clone HMa2; BioLegend), [143]Nd-conjugated CD11c (clone N418; BioLegend), [144]Nd-conjugated CD43 (clone S7; BD Biosciences), [145]Nd-conjugated pSTAT3 (clone Tyr705; BioLegend), [146]Nd-conjugated CD23 (clone B3B4; BioLegend), [147]Sm-conjugated PDL1 (clone 10F.9G2; BioLegend), [148]Sm-conjugated PDCA1 (clone 129c1; BioLegend), [149]Sm-conjugated Siglec-F (clone E50-2440; BD Biosciences), [150]Nd-conjugated pSTAT1 (clone A17012A; BioLegend), [151]Eu-conjugated GL7 (clone GL-7; BioLegend), [152]Sm-conjugated Ki67 (clone SolA15; Invitrogen), [153]Eu-conjugated CD11b (clone M1/70; UCSF), [154]Sm-conjugated Ly6c (clone HK1.4; BioLegend), [155]Gd-conjugated CD8 (clone 53-6.7; BioLegend), [156]Gd-conjugated CD4 (clone RM4-5; BioLegend), [157]Gd-conjugated CD3 (clone 17A2; BioLegend), [158]Gd-conjugated B220 (clone RA3.3A1/6.1; UCSF), [159]Tb-conjugated pSTAT5 (clone pY694; BD Biosciences), [160]Gd-conjugated CD62L-FITC (clone MEL-14; BioLegend), [161]Dy-conjugated T-bet (clone 4B10; BioLegend), [162]Dy-conjugated CD25 (clone PC61; BioLegend), [163]Dy-conjugated Bcl6 (clone IG191E/A8; BioLegend), [164]Dy-conjugated CD86 (clone GL-1; BioLegend), [165]Ho-conjugated CD69 (clone polyclonal; R&D Systems), [166]Er-conjugated MHC II (I-Ad; clone 39-10-8; BioLegend), [167]Er-conjugated FoxP3 (clone NRRF-30; Invitrogen), [168]Er-conjugated RORγt (clone B2D; Invitrogen), [169]Tm-conjugated CTLA4 (clone UC10-4B9; BioLegend), [170]Er-conjugated pSTAT4 (clone Stat4Y693-F6; Invitrogen), [171]Yb-conjugated PD1 (clone RMP1-30; BioLegend), [172]Tb-conjugated GATA3 (clone 16E10A23; BioLegend), [174]Yb-conjugated glucagon (clone U16-850; BD Biosciences), [175]Lu-conjugated CD44 (clone IM7; BioLegend), and [176]Yb-conjugated insulin (clone T56-706; BD Biosciences).

Bone marrow chimeras

Bone marrow was removed from 4–8-wk-old nondiabetic, CD45.2 congenically labeled donor mice, filtered through a 70-mm filter, centrifuged, and resuspended in sterile PBS to a concentration of 10^7 live cells per 200 μl. CD45.1 congenically labeled female NOD recipient mice were lethally irradiated (1,200 rad) 8–16 h before bone marrow transplant. A single-cell suspension of CD45.2 bone marrow in sterile PBS (10^7 live cells per recipient mouse) was transplanted into each recipient mouse by i.v. tail injection. Reconstitution was confirmed by flow cytometry of the peripheral blood at 4–8 wk after transplant. Nonfasting blood glucose levels in recipient mice were monitored weekly by using an Accu-Check glucometer (Roche Diagnostic Corp.). Diabetes onset was considered to have occurred when nonfasting blood glucose concentration exceeded 250 mg/dl for 2 d consecutively.

In vivo T reg suppression assay

NOD.BDC2.5[+] and NOD.BDC2.5^{+}STAT3[+/K392R] lymphocyte single-cell suspensions were made from axillary, inguinal, mesenteric, and para-aortic LNs, as discussed above. CD4^{+}CD25^{+}CD62L^{+} T reg cells and CD4^{+}CD25-CD62L^{+} Teff cells were isolated by cell sorting using a FACSAria sorter before being incubated in ex vivo cultures at 37°C for 10 d. 25–50 × 10^3 purified cells were plated on a 96-well U-bottomed plate, stimulated with mouse anti-CD3/CD28 Dynabeads (3:1 bead-to-cell ratio; Thermo Fisher Scientific), and supplemented with complete medium consisting of DMEM containing 10% heat-inactivated FBS (Biosource International), 5 μM Hepes, nonessential amino acids, 0.5 mM sodium pyruvate, 1 mM GlutaMAX I (all from Invitrogen), penicillin-streptomycin, recombinant human IL-2 (2,000 IU/ml for T reg cell cultures and 200 IU/ml for Teff cell cultures; Prometheus Laboratories), and 55 μM 2-ME (Sigma-Aldrich). On day 10 of ex vivo culture, 5 × 10^6 expanded NOD.BDC2.5[+] or NOD.BDC2.5[+]STAT3[+/K392R] T reg cells along with 5 × 10^6 NOD.BDC2.5^{+} Teff cells were harvested, washed twice, rested in complete media without any IL-2 supplementation for 6 h at 37°C, and resuspended in 100 μl PBS before the individual cell suspensions were injected i.v. via the retroorbital vein into anesthetized NOD.Rag2^{−/−} mice. Successful i.v. infusion was confirmed by direct visualization and palpation of the periorbital area. Nonfasting blood glucose levels in recipient mice were monitored daily by using an Accu-Check glucometer (Roche Diagnostic Corp.). Diabetes onset was considered to have occurred when nonfasting blood glucose concentration exceeded 250 mg/dl for 2 d consecutively.

Adoptive transfer of diabetes using 8.3Tg^{+}CD8^{+} T cells

NOD, NOD.8.3Tg^{+}, and NOD.8.3Tg^{+}STAT3[+/K392R] lymphocyte single-cell suspensions were made from non-pLNs and spleens from nondiabetic donors, as discussed above. NOD cells were CD4 enriched using MACS EasySep CD4-negative selection kits (STEMCELL Technologies), and 8.3Tg^{+} cells were naive CD8 enriched using MACS EasySep naive CD8-negative selection kits (STEMCELL Technologies). Aliquots at each step were analyzed to confirm purity. Purified cells were pooled in a 1:2 ratio of naive CD8^{+}8.3Tg^{+} T cells to polyclonal CD4^{+} T cells and retro-orbitally injected at 1.5 × 10^6 cells per recipient NOD.SCID mouse. Nonfasting blood glucose levels in recipient mice were monitored three times per week by using an Accu-Check glucometer (Roche Diagnostic Corp.) from days 7 to 30 after transfer. Diabetes onset was considered to have occurred when nonfasting blood glucose concentration exceeded 250 mg/dl for 2 d consecutively.

CTV labeling and adoptive transfer of T cells

NOD.BDC2.5[+].Foxp3[RFP] nondiabetic mice donated from the Tang Lab at UCSF were used to generate lymphocyte single-cell suspensions from non-pLNs and spleens, as discussed above. CD4^{+}CD62L^{+}Vβ4^{+}Foxp3^{−} cells were isolated by cell sorting using a FACSAria sorter and labeled using the Invitrogen CellTrace Violet Proliferation Kit, and 1.0 × 10^6 CTV-labeled cells were injected i.v. into WT or STAT3[+/K392R] nondiabetic recipients. 3.5 d after adoptive transfer, pLNs and iLNs were removed and

analyzed for the presence of CTV-labeled cells to assess cell proliferation.

scRNA-seq library preparation and sequencing

Islets were purified following standard collagenase protocols as described previously (Tang et al., 2004) and dissociated by incubating with a nonenzymatic solution (Sigma-Aldrich) followed by trituration per the manufacturer's instructions. After live CD45+ cells were isolated by cell sorting using a FACSAria sorter, cells were spun down and resuspended in PBS. Prior to loading on the 10x Genomics Chromium instrument, cells were counted using a hemocytometer, and the concentration of cells was adjusted to $\sim 10^3$ cells μl^{-1}. A viability of at least 90% for all samples was confirmed by trypan blue staining. Samples were handled on ice when possible. Cells were then processed by the UCSF Immunology Core facility using the Chromium Single Cell 5′ Library and the Gel Bead Kit following the manufacturer's user guide (10x Genomics; CG000086_SingleCellVDJReagentKits-UserGuide_RevB). Single-cell libraries were sequenced on a NovaSeq S4 Flow Cell PE 2 × 150.

scRNA-seq analysis

Reads were processed and aligned to the mm10 reference genome assembly using the 10x Genomics Cell Ranger count pipeline. Doublets were assessed using the R implementation of scrublet (Wolock et al., 2019), "rscrublet." Seurat objects for each sample were created and merged. Barcodes with a doublet score >0.15 and mitochondrial reads >5% or <200 features were removed.

Preprocessing, clustering, and dimensionality reduction were performed using Seurat (Stuart et al., 2019). Clusters were identified using marker genes, including *Cd3e*, *Cd19*, and *Itgax*. T cell clusters 1, 2, and 3 were selected for reclustering and were subsequently reprocessed using the same procedure. A small number of additional contaminants (doublets and non-T cells) were identified and removed. Differential genes were determined with Seurat's "FindAllMarkers" and "FindMarkers" functions and represented as heatmaps (plotted with "pheatmap") or volcano plots (plotted with "ggplot2"). For clarity, ribosomal genes, mitochondrial genes, genes starting with "Gm," and genes ending with "Rik" are not shown in the volcano plots.

Single-cell TCR analysis

TCR sequences were aligned to the mm10 reference genome using the 10x Genomics Cell Ranger V(D)J pipeline. High-confidence clonotypes for each sample were merged to obtain a single clone identification by matching identical CDR3 amino acid sequences between the samples. These merged clones were added to the Seurat object metadata for downstream analysis.

scATAC-seq library preparation and sequencing

Cells were processed using the 10x Genomics single-cell ATAC reagents and protocols as described previously (Satpathy et al., 2019). Briefly, bulk cells were transposed, single cells were loaded into droplets for barcoding using the 10x Genomics Chromium platform, and then DNA was amplified and prepared for sequencing. Libraries were sequenced at the Stanford Functional Genomics Facility.

Single-cell ATAC analysis

Reads were processed and aligned to the mm10 reference genome assembly using the 10x Genomics Cell Ranger ATAC count pipeline. Fragment files were loaded into ArchR for all downstream analysis (Granja et al., 2021). ArchR default settings were used for doublet calling, quality filtering (based on transcription start site enrichment and number of fragments per cell), and computing the cell by tile matrix.

The tile matrix was used for dimensionality reduction and clustering of the cells. ArchR gene scores were used to determine cluster identities, and T cells were selected for reclustering, analogous to the scRNA workflow. ArchR was then used to create a cell-by-peak matrix and cell-by-motif deviation matrix. Markers for each matrix were determined using the "getMarkerFeatures" utility and then displayed via heatmap or volcano plot. Accessibility for selected genomic regions was visualized using the ArchR browser, where each track for a particular region is shown on the same fixed scale and normalized by reads in transcription start sites genome-wide.

Histology

Pancreata were removed and fixed in 10% neutral-buffered formalin (Sigma-Aldrich). Paraffin-embedded step sections were stained with H&E, and insulitis was scored as described previously (Katz et al., 1993).

Immunofluorescence

For immunofluorescence, pancreata were fixed in 2% paraformaldehyde (Pierce) in PBS for 2 h at 4°C followed by overnight incubation in 30% (wt/vol) sucrose (Sigma-Aldrich) in PBS. Tissues were embedded in optimum cutting temperature compound (Tissue-Tek) and stored at –80°C before sectioning (50–200 μm) on a cryostat (Leica). Thin sections were dried on Superfrost Plus (Fisher Scientific) slides, and semithick (200 μm) sections were moved directly to 0.3% Triton X-100 (Sigma-Aldrich), 0.2% BSA (Sigma-Aldrich), and 0.1% sodium azide (Sigma-Aldrich) in PBS (Immunomix). Slides were stained in a humidified chamber, and semithick sections were stained in 24-well plates with one section per well. Slides were briefly rehydrated in PBS before permeabilization in Immunomix for 1 h at RT followed by blocking with BlockAid (Thermo Fisher Scientific); primary antibody staining at RT; and, when necessary, secondary antibody staining at RT for 1 h. Semithick sections were permeabilized in Immunomix with shaking at RT overnight followed by blocking with BlockAid at RT for 2 h; primary antibody staining at RT for 2 h; and, when necessary, secondary antibody staining at RT for 2 h. Semithick sections were then moved to Superfrost Plus slides, and all sections were mounted with ProLong Diamond Antifade Mountant (Thermo Fisher Scientific). Images were acquired on a Leica SP5 (Leica) laser scanning confocal microscope.

Statistical analysis

All experiments were performed using randomly assigned mice without investigator blinding. No data were excluded. Statistical significance between two groups was calculated using an unpaired, parametric, two-tailed Student's *t* test. Experimental

Warshauer et al.
STAT3-GOF disrupts CD8 tolerance to promote T1D

Journal of Experimental Medicine   12 of 15
https://doi.org/10.1084/jem.20210759

groups included a minimum of three biological replicates. Intragroup variation was not assessed. All statistical analysis was performed using Prism 7 (GraphPad Software). Figures display mean ± SD values. A P value <0.05 was considered statistically significant. No statistical methods were used to predetermine sample size.

Online supplemental material

Fig. S1 provides additional characterization of the STAT3$^{+/-}$ ^{K392R} diabetic phenotype. Fig. S2 provides detailed analyses of scRNA-seq data. Fig. S3 provides detailed analyses of scATAC-seq data, scTCR-seq data, and additional adoptive T cell transfer experiments.

Data availability

Sequence data that support the findings of this study have been deposited in the Gene Expression Omnibus database under accession no. GSE173415.

References

Abdelsamed, H.A., C.C. Zebley, H. Nguyen, R.L. Rutishauser, Y. Fan, H.E. Ghoneim, J.C. Crawford, F. Alfei, S. Alli, S.P. Ribeiro, et al. 2020. Beta cell-specific CD8$^+$ T cells maintain stem cell memory-associated epigenetic programs during type 1 diabetes. *Nat. Immunol.* 21:578–587. https://doi.org/10.1038/s41590-020-0633-5

Ansari, M.J., A.D. Salama, T. Chitnis, R.N. Smith, H. Yagita, H. Akiba, T. Yamazaki, M. Azuma, H. Iwai, S.J. Khoury, et al. 2003. The programmed death-1 (PD-1) pathway regulates autoimmune diabetes in nonobese diabetic (NOD) mice. *J. Exp. Med.* 198:63–69. https://doi.org/10.1084/jem.20022125

Beltra, J.C., S. Manne, M.S. Abdel-Hakeem, M. Kurachi, J.R. Giles, Z. Chen, V. Casella, S.F. Ngiow, O. Khan, Y.J. Huang, et al. 2020. Developmental relationships of four exhausted CD8$^+$ T cell subsets reveals underlying transcriptional and epigenetic landscape control mechanisms. *Immunity.* 52:825–841.e8. https://doi.org/10.1016/j.immuni.2020.04.014

Buckner, J.H., and G.T. Nepom. 2016. Obstacles and opportunities for targeting the effector T cell response in type 1 diabetes. *J. Autoimmun.* 71: 44–50. https://doi.org/10.1016/j.jaut.2016.02.009

Christianson, S.W., L.D. Shultz, and E.H. Leiter. 1993. Adoptive transfer of diabetes into immunodeficient NOD-scid/scid mice. Relative contributions of CD4$^+$ and CD8$^+$ T-cells from diabetic versus prediabetic NOD.NON-Thy-1a donors. *Diabetes.* 42:44–55. https://doi.org/10.2337/diab.42.1.44

Ciucci, T., M.S. Vacchio, and R. Bosselut. 2017. A STAT3-dependent transcriptional circuitry inhibits cytotoxic gene expression in T cells. *Proc. Natl. Acad. Sci. USA.* 114:13236–13241. https://doi.org/10.1073/pnas.1711160114

Cui, W., Y. Liu, J.S. Weinstein, J. Craft, and S.M. Kaech. 2011. An interleukin-21-interleukin-10-STAT3 pathway is critical for functional maturation of memory CD8$^+$ T cells. *Immunity.* 35:792–805. https://doi.org/10.1016/j.immuni.2011.09.017

De Leenheer, E., and F.S. Wong. 2015. Adoptive transfer of autoimmune diabetes using immunodeficient nonobese diabetic (NOD) mice. *Methods Mol. Biol.* 1433:135–140. https://doi.org/10.1007/7651_2015_294

Durant, L., W.T. Watford, H.L. Ramos, A. Laurence, G. Vahedi, L. Wei, H. Takahashi, H.W. Sun, Y. Kanno, F. Powrie, and J.J. O'Shea. 2010. Diverse targets of the transcription factor STAT3 contribute to T cell pathogenicity and homeostasis. *Immunity.* 32:605–615. https://doi.org/10.1016/j.immuni.2010.05.003

Erlich, H., A.M. Valdes, J. Noble, J.A. Carlson, M. Varney, P. Concannon, J.C. Mychaleckyj, J.A. Todd, P. Bonella, A.L. Fear, et al. Type 1 Diabetes Genetics Consortium. 2008. HLA DR-DQ haplotypes and genotypes and type 1 diabetes risk: analysis of the type 1 diabetes genetics consortium families. *Diabetes.* 57:1084–1092. https://doi.org/10.2337/db07-1331

Fabbri, M., M. Frixou, M. Degano, and G. Fousteri. 2019. Type 1 diabetes in STAT protein family mutations: regulating the Th17/Treg equilibrium and beyond. *Diabetes.* 68:258–265. https://doi.org/10.2337/db18-0627

Faletti, L., S. Ehl, and M. Heeg. 2021. Germline STAT3 gain-of-function mutations in primary immunodeficiency: impact on the cellular and clinical phenotype. *Biomed. J.* https://doi.org/10.1016/j.bj.2021.03.003

Ferreira, R.C., D.F. Freitag, A.J. Cutler, J.M. Howson, D.B. Rainbow, D.J. Smyth, S. Kaptoge, P. Clarke, C. Boreham, R.M. Coulson, et al. 2013. Functional IL6R 358Ala allele impairs classical IL-6 receptor signaling and influences risk of diverse inflammatory diseases. *PLoS Genet.* 9: e1003444. https://doi.org/10.1371/journal.pgen.1003444

Finck, R., E.F. Simonds, A. Jager, S. Krishnaswamy, K. Sachs, W. Fantl, D. Pe'er, G.P. Nolan, and S.C. Bendall. 2013. Normalization of mass cytometry data with bead standards. *Cytometry A.* 83:483–494. https://doi.org/10.1002/cyto.a.22271

Flanagan, S.E., E. Haapaniemi, M.A. Russell, R. Caswell, H.L. Allen, E. De Franco, T.J. McDonald, H. Rajala, A. Ramelius, J. Barton, et al. 2014. Activating germline mutations in STAT3 cause early-onset multi-organ autoimmune disease. *Nat. Genet.* 46:812–814. https://doi.org/10.1038/ng.3040

Fung, E.Y.M.G., D.J. Smyth, J.M.M. Howson, J.D. Cooper, N.M. Walker, H. Stevens, L.S. Wicker, and J.A. Todd. 2009. Analysis of 17 autoimmune disease-associated variants in type 1 diabetes identifies 6q23/*TNFAIP3* as a susceptibility locus. *Genes Immun.* 10:188–191. https://doi.org/10.1038/gene.2008.99

Gepts, W. 1965. Pathologic anatomy of the pancreas in juvenile diabetes mellitus. *Diabetes.* 14:619–633. https://doi.org/10.2337/diab.14.10.619

Gepts, W., and J. De Mey. 1978. Islet cell survival determined by morphology. An immunocytochemical study of the islets of Langerhans in juvenile diabetes mellitus. *Diabetes.* 27(Suppl 1):251–261. https://doi.org/10.2337/diab.27.1.S251

Gorogawa, S., Y. Fujitani, H. Kaneto, Y. Hazama, H. Watada, Y. Miyamoto, K. Takeda, S. Akira, M.A. Magnuson, Y. Yamasaki, et al. 2004. Insulin secretory defects and impaired islet architecture in pancreatic beta-cell-specific STAT3 knockout mice. *Biochem. Biophys. Res. Commun.* 319: 1159–1170. https://doi.org/10.1016/j.bbrc.2004.05.095

Granja, J.M., M.R. Corces, S.E. Pierce, S.T. Bagdatli, H. Choudhry, H.Y. Chang, and W.J. Greenleaf. 2021. ArchR is a scalable software package for integrative single-cell chromatin accessibility analysis. *Nat. Genet.* 53: 403–411. https://doi.org/10.1038/s41588-021-00790-6

Herold, K.C., B.N. Bundy, S.A. Long, J.A. Bluestone, L.A. DiMeglio, M.J. Dufort, S.E. Gitelman, P.A. Gottlieb, J.P. Krischer, P.S. Linsley, et al. Type 1 Diabetes TrialNet Study Group. 2019. An anti-CD3 antibody, teplizumab, in relatives at risk for type 1 diabetes. *N. Engl. J. Med.* 381:603–613. https://doi.org/10.1056/NEJMoa1902226

Hudson, W.H., J. Gensheimer, M. Hashimoto, A. Wieland, R.M. Valanparambil, P. Li, J.-X. Lin, B.T. Konieczny, S.J. Im, G.J. Freeman, et al. 2019. Proliferating transitory T cells with an effector-like transcriptional signature emerge from PD-1^{+} stem-like CD8^{+} T cells during chronic infection. *Immunity.* 51:1043–1058.e4. https://doi.org/10.1016/j.immuni.2019.11.002

Hundhausen, C., A. Roth, E. Whalen, J. Chen, A. Schneider, S.A. Long, S. Wei, R. Rawlings, M. Kinsman, S.P. Evanko, et al. 2016. Enhanced T cell responses to IL-6 in type 1 diabetes are associated with early clinical disease and increased IL-6 receptor expression. *Sci. Transl. Med.* 8: 356ra119. https://doi.org/10.1126/scitranslmed.aad9943

Ihantola, E.-L., T. Viisanen, A.M. Gazali, K. Näntö-Salonen, A. Juutilainen, L. Moilanen, R. Rintamäki, J. Pihlajamäki, R. Veijola, J. Toppari, et al. 2018. Effector T cell resistance to suppression and STAT3 signaling during the development of human type 1 diabetes. *J. Immunol.* 201:1144–1153. https://doi.org/10.4049/jimmunol.1701199

Im, S.J., M. Hashimoto, M.Y. Gerner, J. Lee, H.T. Kissick, M.C. Burger, Q. Shan, J.S. Hale, J. Lee, T.H. Nasti, et al. 2016. Defining CD8^{+} T cells that provide the proliferative burst after PD-1 therapy. *Nature.* 537:417–421. https://doi.org/10.1038/nature19330

Jun, H.S., P. Santamaria, H.W. Lim, M.L. Zhang, and J.W. Yoon. 1999. Absolute requirement of macrophages for the development and activation of beta-cell cytotoxic CD8^{+} T-cells in T-cell receptor transgenic NOD mice. *Diabetes.* 48:34–42. https://doi.org/10.2337/diabetes.48.1.34

June, C.H., J.T. Warshauer, and J.A. Bluestone. 2017. Is autoimmunity the Achilles' heel of cancer immunotherapy? *Nat. Med.* 23:540–547. https://doi.org/10.1038/nm.4321

Kaech, S.M., and W. Cui. 2012. Transcriptional control of effector and memory CD8^{+} T cell differentiation. *Nat. Rev. Immunol.* 12:749–761. https://doi.org/10.1038/nri3307

Katz, J.D., B. Wang, K. Haskins, C. Benoist, and D. Mathis. 1993. Following a diabetogenic T cell from genesis through pathogenesis. *Cell.* 74: 1089–1100. https://doi.org/10.1016/0092-8674(93)90730-E

Keir, M.E., S.C. Liang, I. Guleria, Y.E. Latchman, A. Qipo, L.A. Albacker, M. Koulmanda, G.J. Freeman, M.H. Sayegh, and A.H. Sharpe. 2006. Tissue expression of PD-L1 mediates peripheral T cell tolerance. *J. Exp. Med.* 203:883–895. https://doi.org/10.1084/jem.20051776

Kotecha, N., P.O. Krutzik, and J.M. Irish. 2010. Web-based analysis and publication of flow cytometry experiments. Curr. Protoc. Cytom. Chapter 10:Unit10.17.

Levine, L., K. Hiam, D. Marquez, I. Tenvooren, D. Contreras, J. Rathmell, and M. Spitzer. 2020. Single-cell metabolic analysis by mass cytometry reveals distinct transitional states of CD8 T cell differentiation [abstract]. *J. Immunol.* 204:155.18.

Long, S.A., J. Thorpe, H.A. DeBerg, V. Gersuk, J. Eddy, K.M. Harris, M. Ehlers, K.C. Herold, G.T. Nepom, and P.S. Linsley. 2016. Partial exhaustion of CD8 T cells and clinical response to teplizumab in new-onset type 1 diabetes. *Sci. Immunol.* 1:eaai7793. https://doi.org/10.1126/sciimmunol.aai7793

Madisen, L., T.A. Zwingman, S.M. Sunkin, S.W. Oh, H.A. Zariwala, H. Gu, L.L. Ng, R.D. Palmiter, M.J. Hawrylycz, A.R. Jones, et al. 2010. A robust and high-throughput Cre reporting and characterization system for the whole mouse brain. *Nat. Neurosci.* 13:133–140. https://doi.org/10.1038/nn.2467

Maffucci, P., C.A. Filion, B. Boisson, Y. Itan, L. Shang, J.L. Casanova, and C. Cunningham-Rundles. 2016. Genetic diagnosis using whole exome sequencing in common variable immunodeficiency. *Front. Immunol.* 7: 220. https://doi.org/10.3389/fimmu.2016.00220

Marwaha, A.K., S.Q. Crome, C. Panagiotopoulos, K.B. Berg, H. Qin, Q. Ouyang, L. Xu, J.J. Priatel, M.K. Levings, and R. Tan. 2010. Cutting edge: Increased IL-17-secreting T cells in children with new-onset type 1 diabetes. *J. Immunol.* 185:3814–3818. https://doi.org/10.4049/jimmunol.1001860

McKinney, E.F., J.C. Lee, D.R. Jayne, P.A. Lyons, and K.G. Smith. 2015. T-cell exhaustion, co-stimulation and clinical outcome in autoimmunity and infection. *Nature.* 523:612–616. https://doi.org/10.1038/nature14468

Milner, J.D., T.P. Vogel, L. Forbes, C.A. Ma, A. Stray-Pedersen, J.E. Niemela, J.J. Lyons, K.R. Engelhardt, Y. Zhang, N. Topcagic, et al. 2015. Early-onset lymphoproliferation and autoimmunity caused by germline STAT3 gain-of-function mutations. *Blood.* 125:591–599. https://doi.org/10.1182/blood-2014-09-602763

Milner, J.J., C. Toma, B. Yu, K. Zhang, K. Omilusik, A.T. Phan, D. Wang, A.J. Getzler, T. Nguyen, S. Crotty, et al. 2017. Runx3 programs CD8^{+} T cell residency in non-lymphoid tissues and tumours. *Nature.* 552:253–257. https://doi.org/10.1038/nature24993

Nabhani, S., C. Schipp, H. Miskin, C. Levin, S. Postovsky, T. Dujovny, A. Koren, D. Harlev, A.M. Bis, F. Auer, et al. 2017. STAT3 gain-of-function mutations associated with autoimmune lymphoproliferative syndrome like disease deregulate lymphocyte apoptosis and can be targeted by BH3 mimetic compounds. *Clin. Immunol.* 181:32–42. https://doi.org/10.1016/j.clim.2017.05.021

O'Shea, J.J., and R. Plenge. 2012. JAK and STAT signaling molecules in immunoregulation and immune-mediated disease. *Immunity.* 36:542–550. https://doi.org/10.1016/j.immuni.2012.03.014

Saarimäki-Vire, J., D. Balboa, M.A. Russell, J. Saarikettu, M. Kinnunen, S. Keskitalo, A. Malhi, C. Valensisi, C. Andrus, S. Eurola, et al. 2017. An activating STAT3 mutation causes neonatal diabetes through premature induction of pancreatic differentiation. *Cell Rep.* 19:281–294. https://doi.org/10.1016/j.celrep.2017.03.055

Satpathy, A.T., J.M. Granja, K.E. Yost, Y. Qi, F. Meschi, G.P. McDermott, B.N. Olsen, M.R. Mumbach, S.E. Pierce, M.R. Corces, et al. 2019. Massively parallel single-cell chromatin landscapes of human immune cell development and intratumoral T cell exhaustion. *Nat. Biotechnol.* 37: 925–936. https://doi.org/10.1038/s41587-019-0206-z

Schep, A.N., B. Wu, J.D. Buenrostro, and W.J. Greenleaf. 2017. chromVAR: inferring transcription-factor-associated accessibility from single-cell epigenomic data. *Nat. Methods.* 14:975–978. https://doi.org/10.1038/nmeth.4401

Sediva, H., P. Dusatkova, V. Kanderova, B. Obermannova, J. Kayserova, L. Sramkova, D. Zemkova, L. Elblova, M. Svaton, R. Zachova, et al. 2017. Short stature in a boy with multiple early-onset autoimmune conditions due to a STAT3 activating mutation: could intracellular growth hormone signalling be compromised? *Horm. Res. Paediatr.* 88:160–166. https://doi.org/10.1159/000456544

Sharma, A., X. Liu, D. Hadley, W. Hagopian, W.M. Chen, S. Onengut-Gumuscu, C. Törn, A.K. Steck, B.I. Frohnert, M. Rewers, et al. TEDDY Study Group. 2018. Identification of non-HLA genes associated with development of islet autoimmunity and type 1 diabetes in the prospective TEDDY cohort. *J. Autoimmun.* 89:90–100. https://doi.org/10.1016/j.jaut.2017.12.008

Siddiqui, I., K. Schaeuble, V. Chennupati, S.A. Fuertes Marraco, S. Calderon-Copete, D. Pais Ferreira, S.J. Carmona, L. Scarpellino, D. Gfeller, S. Pradervand, et al. 2019. Intratumoral Tcf1+PD-1+CD8+ T cells with stem-like properties promote tumor control in response to vaccination and checkpoint blockade immunotherapy. *Immunity.* 50:195–211.e10. https://doi.org/10.1016/j.immuni.2018.12.021

Sims, E.K., B.N. Bundy, K. Stier, E. Serti, N. Lim, S.A. Long, S.M. Geyer, A. Moran, C.J. Greenbaum, C. Evans-Molina, and K.C. Herold. Type 1 Diabetes TrialNet Study Group. 2021. Teplizumab improves and stabilizes beta cell function in antibody-positive high-risk individuals. *Sci. Transl. Med.* 13:eabc8980. https://doi.org/10.1126/scitranslmed.abc8980

Stadinski, B.D., T. Delong, N. Reisdorph, R. Reisdorph, R.L. Powell, M. Armstrong, J.D. Piganelli, G. Barbour, B. Bradley, F. Crawford, et al. 2010. Chromogranin A is an autoantigen in type 1 diabetes. *Nat. Immunol.* 11:225–231. https://doi.org/10.1038/ni.1844

Stuart, T., A. Butler, P. Hoffman, C. Hafemeister, E. Papalexi, W.M. Mauck III, Y. Hao, M. Stoeckius, P. Smibert, and R. Satija. 2019. Comprehensive integration of single-cell data. *Cell.* 177:1888–1902.e21. https://doi.org/10.1016/j.cell.2019.05.031

Tang, Q., K.J. Henriksen, M. Bi, E.B. Finger, G. Szot, J. Ye, E.L. Masteller, H. McDevitt, M. Bonyhadi, and J.A. Bluestone. 2004. In vitro-expanded antigen-specific regulatory T cells suppress autoimmune diabetes. *J. Exp. Med.* 199:1455–1465. https://doi.org/10.1084/jem.20040139

Tarbell, K.V., S. Yamazaki, K. Olson, P. Toy, and R.M. Steinman. 2004. CD25+ CD4+ T cells, expanded with dendritic cells presenting a single autoantigenic peptide, suppress autoimmune diabetes. *J. Exp. Med.* 199:1467–1477. https://doi.org/10.1084/jem.20040180

Velayos, T., R. Martínez, M. Alonso, K. Garcia-Etxebarria, A. Aguayo, C. Camarero, I. Urrutia, I. Martínez de LaPiscina, R. Barrio, I. Santin, and L. Castaño. 2017. An activating mutation in *STAT3* results in neonatal diabetes through reduced insulin synthesis. *Diabetes.* 66:1022–1029. https://doi.org/10.2337/db16-0867

Verdaguer, J., D. Schmidt, A. Amrani, B. Anderson, N. Averill, and P. Santamaria. 1997. Spontaneous autoimmune diabetes in monoclonal T cell nonobese diabetic mice. *J. Exp. Med.* 186:1663–1676. https://doi.org/10.1084/jem.186.10.1663

Viisanen, T., E.-L. Ihantola, K. Näntö-Salonen, H. Hyöty, N. Nurminen, J. Selvenius, A. Juutilainen, L. Moilanen, J. Pihlajamäki, R. Veijola, et al. 2017. Circulating CXCR5+PD-1+ICOS+ follicular T Helper cells are increased close to the diagnosis of type 1 diabetes in children with multiple autoantibodies. *Diabetes.* 66:437–447. https://doi.org/10.2337/db16-0714

Wang, J., L. Liu, J. Ma, F. Sun, Z. Zhao, and M. Gu. 2014. Common variants on cytotoxic T lymphocyte antigen-4 polymorphisms contributes to type 1 diabetes susceptibility: evidence based on 58 studies. *PLoS One.* 9: e85982. https://doi.org/10.1371/journal.pone.0085982

Warshauer, J.T., J.A. Bluestone, and M.S. Anderson. 2020. New frontiers in the treatment of type 1 diabetes. *Cell Metab.* 31:46–61. https://doi.org/10.1016/j.cmet.2019.11.017

Weinreich, M.A., K. Takada, C. Skon, S.L. Reiner, S.C. Jameson, and K.A. Hogquist. 2009. KLF2 transcription-factor deficiency in T cells results in unrestrained cytokine production and upregulation of bystander chemokine receptors. *Immunity.* 31:122–130. https://doi.org/10.1016/j.immuni.2009.05.011

Wiedeman, A.E., V.S. Muir, M.G. Rosasco, H.A. DeBerg, S. Presnell, B. Haas, M.J. Dufort, C. Speake, C.J. Greenbaum, E. Serti, et al. 2020. Autoreactive CD8+ T cell exhaustion distinguishes subjects with slow type 1 diabetes progression. *J. Clin. Invest.* 130:480–490. https://doi.org/10.1172/JCI126595

Wienke, J., W. Janssen, R. Scholman, H. Spits, M. van Gijn, M. Boes, J. van Montfrans, N. Moes, and S. de Roock. 2015. A novel human STAT3 mutation presents with autoimmunity involving Th17 hyperactivation. *Oncotarget.* 6:20037–20042. https://doi.org/10.18632/oncotarget.5042

Wolock, S.L., R. Lopez, and A.M. Klein. 2019. Scrublet: computational identification of cell doublets in single-cell transcriptomic data. *Cell Syst.* 8: 281–291.e9. https://doi.org/10.1016/j.cels.2018.11.005

Wu, T., Y. Ji, E.A. Moseman, H.C. Xu, M. Manglani, M. Kirby, S.M. Anderson, R. Handon, E. Kenyon, A. Elkahloun, et al. 2016. The TCF1-Bcl6 axis counteracts type I interferon to repress exhaustion and maintain T cell stemness. *Sci. Immunol.* 1:eaai8593. https://doi.org/10.1126/sciimmunol.aai8593

Yeo, L., A. Woodwyk, S. Sood, A. Lorenc, M. Eichmann, I. Pujol-Autonell, R. Melchiotti, A. Skowera, E. Fidanis, G.M. Dolton, et al. 2018. Autoreactive T effector memory differentiation mirrors β cell function in type 1 diabetes. *J. Clin. Invest.* 128:3460–3474. https://doi.org/10.1172/JCI120555

Zakharov, P.N., H. Hu, X. Wan, and E.R. Unanue. 2020. Single-cell RNA sequencing of murine islets shows high cellular complexity at all stages of autoimmune diabetes. *J. Exp. Med.* 217:e20192362. https://doi.org/10.1084/jem.20192362

Zunder, E.R., E. Lujan, Y. Goltsev, M. Wernig, and G.P. Nolan. 2015. A continuous molecular roadmap to iPSC reprogramming through progression analysis of single-cell mass cytometry. *Cell Stem Cell.* 16:323–337. https://doi.org/10.1016/j.stem.2015.01.015
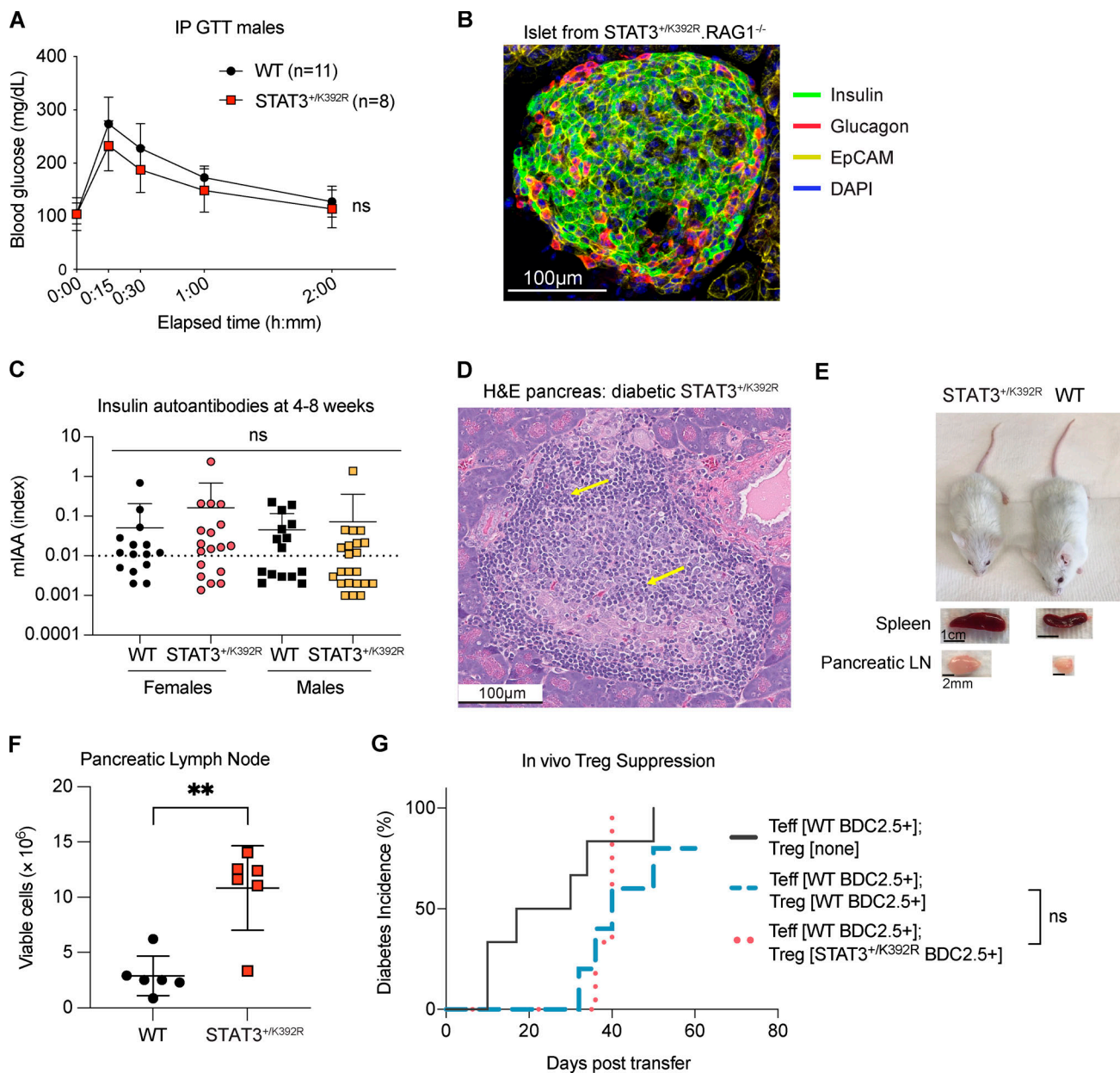
Supplemental material

Figure S1. **Phenotyping of STAT3+/K392R mouse model. (A)** Intraperitoneal glucose tolerance testing (IP GTT) of young (<8 wk of age) WT (*n* = 11) versus STAT3+/K392R (*n* = 8) mice. **(B)** Immunofluorescence of islet in STAT3+/K392R Rag1−/− showing normal distribution of α cells (glucagon+) and β cells (insulin+). Scale bar, 100 μm. EpCAM, epithelial cell adhesion molecule. **(C)** Prevalence of insulin autoantibodies (mIAA) in nondiabetic mice 4–8 wk of age (females: WT, *n* = 20; STAT3+/K392R, *n* = 20; males: WT, *n* = 17; STAT3+/K392R, *n* = 23). **(D)** H&E staining of the pancreas from a diabetic STAT3+/K392R mouse at 13 wk of age showing severe insulitis. Scale bar, 100 μm. Yellow arrows indicate dense lymphocytic infiltrate into the islet. **(E)** Lymphoproliferation in nondiabetic female littermates at 6 wk with spleens and pLNs as representative examples. Scale bar for spleens, 1 cm. Scale bar for pLNs, 2 mm. **(F)** Absolute cell counts in pLNs of WT (*n* = 6) versus STAT3+/K392R (*n* = 6) nondiabetic mice at 7–8 wk of age. P = 0.006. **(G)** In vivo T reg suppression assay showing diabetes incidence after adoptive transfer of WT CD4+BDC2.5+ Teff cells without (*n* = 6) and with T regs from WT (*n* = 5) or STAT3+/K392R (*n* = 3) BDC2.5+ mice into NOD.Rag1−/− mice. Data in A, F, and G are pooled from two independent experiments. Data are shown as mean ± SD. Student's *t* test (A, C, and F) or log-rank (Mantel-Cox) test (G) was used. **, P ≤ 0.01.
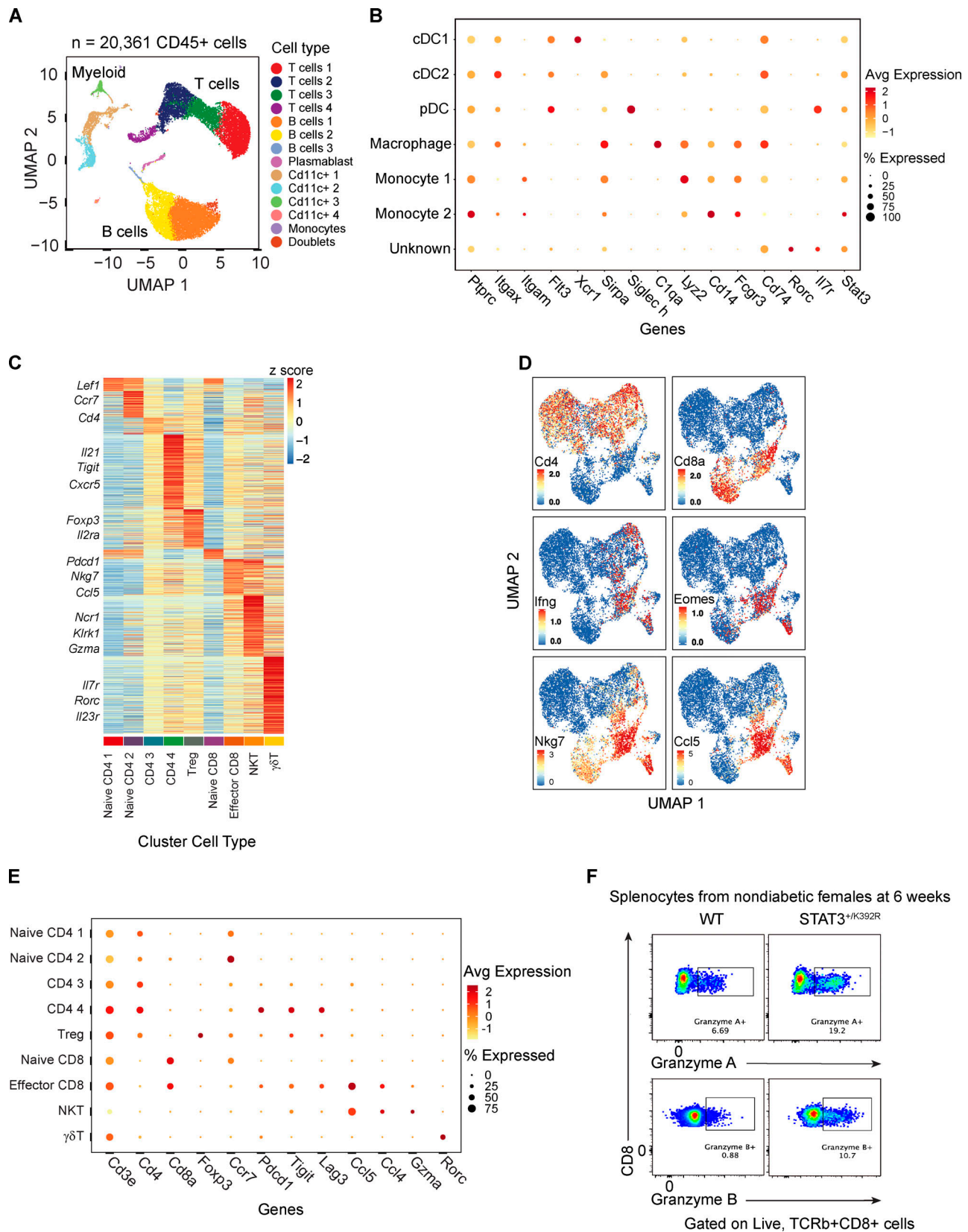
Figure S2. **Additional characterization of scRNA-seq infiltrating islet immune cells. (A)** UMAP projection of scRNA-seq profiles of cells isolated from CD45+ islet infiltrates of 8–10-wk-old male nondiabetic mice, WT (*n* = 3, pooled), and STAT3+/K392R (*n* = 3, pooled). **(B)** Summary of marker genes used to identify APC clusters. **(C)** Additional marker gene characterization for the scRNA-seq T cell clusters. **(D)** Expression of selected genes visualized for each T cell. **(E)** Summary of marker genes used to identify T cell clusters. γδT, γδ T cells. **(F)** Additional flow cytometry data on granzyme A and granzyme B protein expression for both genotypes.
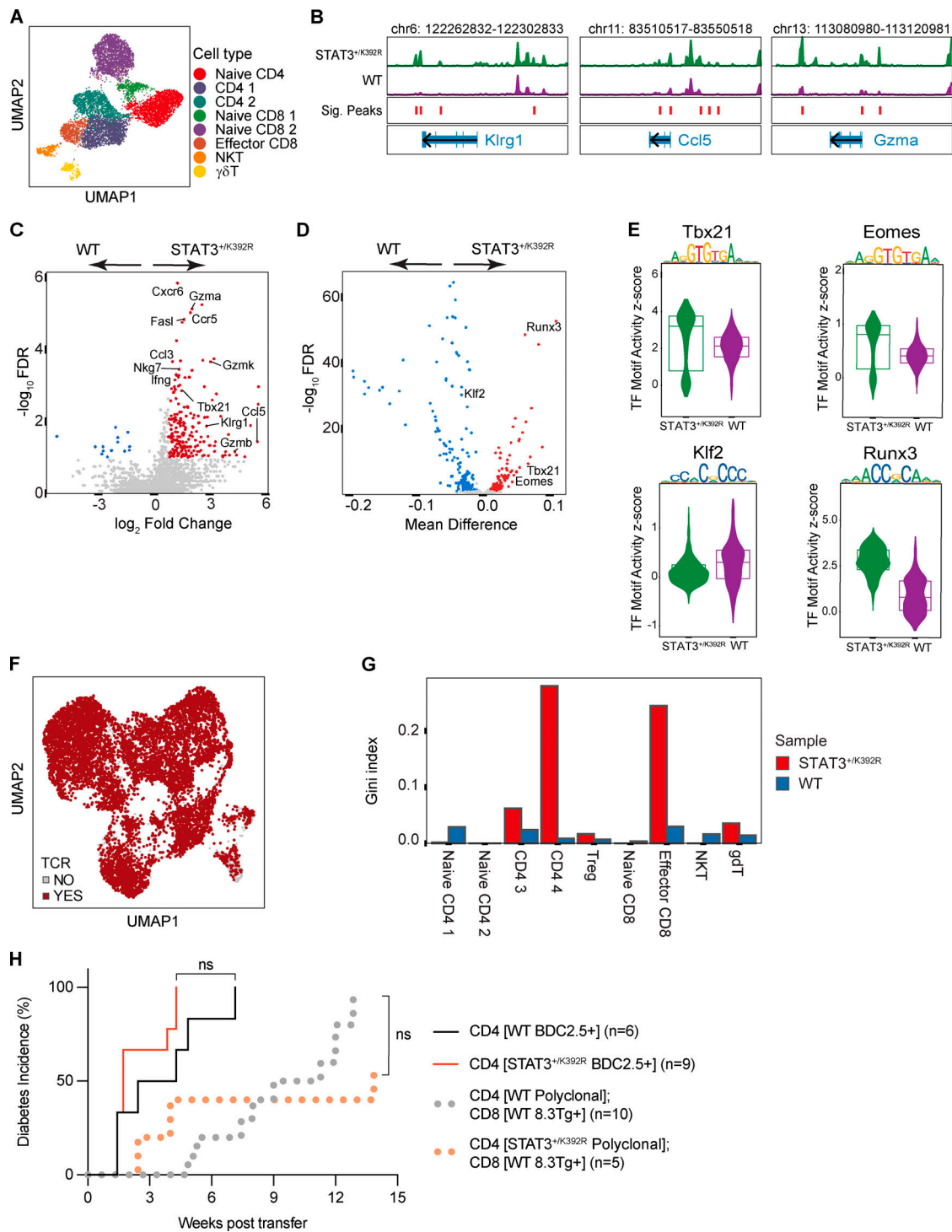
Figure S3. **scATAC-seq of infiltrating islet immune cells, additional characterizations of scTCR-seq data, and functional T cell adoptive transfer experiments. (A)** UMAP projection of scATAC-seq profiles of T cells (CD3⁺) subclustered from CD45⁺ islet infiltrates of 8–10-wk-old male nondiabetic mice, WT (*n* = 3, pooled), and STAT3⁺/K392R (*n* = 3, pooled). γδT, γδ T cells. **(B)** Normalized pseudobulk ATAC-seq tracks of CD8⁺ T cell clusters split by genotype around genes identified as up-regulated in corresponding scRNA-seq CD8⁺ T cell clusters. Peaks significantly up-regulated (from C) are shown in red. **(C)** Volcano plot showing differential peaks whose nearest gene is present in the significantly up-regulated genes (Fig. 4 B) between CD8⁺ T cell clusters (WT versus STAT3⁺/K392R). FDR, false discovery rate. **(D)** Volcano plot showing differential transcription factor motifs between CD8⁺ T cell clusters (WT versus STAT3⁺/K392R). **(E)** Transcription factor motif activity for CD8⁺ T cell clusters split by genotype. Motif sequence is shown above each violin plot. **(F)** TCR expression in UMAP clusters from subset of CD3⁺ T cells identified in scRNA-seq analysis. **(G)** Gini index showing clonal expansion in STAT3⁺/K392R broken down by cluster and genotype. **(H)** Diabetes incidence after adoptive transfer of CD4⁺ BDC2.5⁺ Teff cells from mice without (*n* = 6) and with STAT3⁺/K392R (*n* = 9) into NOD.Rag1⁻/⁻ mice (solid lines) and diabetes incidence after adoptive transfer of naive CD8⁺ T cells from WT 8.3Tg⁺ mice with polyclonal CD4⁺ T cells from mice without (*n* = 10) and with STAT3⁺/K392R (*n* = 5) into NOD.SCID mice (dotted lines). Results are pooled from two independent experiments for each set of incidence curves (solid lines and dotted lines), and a log-rank (Mantel-Cox) test was used.